PHOTON-INDUCED VORTEX-ANTIVORTEX PAIR CREATION IN SUPERCONDUCTING FILMS

BY

JOSEPH PHILIP WALKO II

B.A., Potsdam College of the State University of New York, 1987
M.S., University of Illinois at Urbana-Champaign, 1990

THESIS

Submitted in partial fulfillment of the requirements
for the degree of Doctor of Philosophy in Physics
in the Graduate College of the
University of Illinois at Urbana-Champaign, 1995

Urbana, Illinois

UNIVERSITY OF ILLINOIS AT URBANA-CHAMPAIGN

THE GRADUATE COLLEGE

February 20, 1995

WE HEREBY RECOMMEND THAT THE THESIS BY

Joseph Philip Walko II

ENTITLED Magnetic Photoresponse in Thin Film Superconductors

BE ACCEPTED IN PARTIAL FULFILLMENT OF THE REQUIREMENTS FOR

THE DEGREE OF Doctor of Philosophy

Director of Thesis Research

Head of Department

Committee on Final Examination†

Chairperson

† Required for doctor's degree but not for master's

O 517

PHOTON-INDUCED VORTEX-ANTIVORTEX PAIR CREATION IN SUPERCONDUCTING FILMS

Joseph Philip Walko II, Ph.D.
Department of Physics and Materials Research Laboratory
University of Illinois at Urbana-Champaign, 1995
Dale VanHarlingen, Advisor

We have used a dc SQUID (Superconducting Quantum Interference Device) to study vortex-antivortex pair creation in both two-dimensional superconducting films and Josephson junction arrays in the presence of 850 nm light irradiation. Specifically the experiments aim to distinguish between the formation of vortex-antivortex pairs by single photon absorption and by thermal activation. The major objective for this experiment is to investigate the possibility of photon-induced vortex-antivortex pair creation.

To my parents

ACKNOWLEDGMENTS

A king's secret it is prudent to keep, but the works
of God are to be declared and made known.
Praise them with due honor.
-- Tobit 12:7

First of all, I would like to thank and praise God, who has brought me here and saw that this work was carried out. I would also like to thank the community of St. John's Catholic Chapel, whose words and lives have taught me how to be alive, showed me true love and true joy, and showed me how to approach my research.

I would like to express my appreciation to Prof. D.J. VanHarlingen for the support, enthusiasm, and patience that he gave throughout the course of this research. I would also like to thank my co-workers for their helpful discussions and assistance.

In addition Prof. Mohammed Abdul Islam provided excellent experience in the undergraduate research at Potsdam College and Dr. Meyer at Burnt Hills-Ballston Lake High School provided an excellent introduction to physics and how it should be approached. He also was very patient with students who were late to class.

In addition I would like to thank my wife Audrey for her patience and support over the last two years, and my parents for their love and support over the last 29.

Finally, I would like to thank the taxpayers of the United States of America for seeing fit to fund my graduate education. This work was supported by the National Science Foundation under Materials Research Laboratory Grant No. NSF-DMR89-20538.

TABLE OF CONTENTS

I. INTRODUCTION

1: Background

Many researchers have produced voltages across current carrying superconducting films by exposing these films to visible and infrared radiation. The most straightforward effect of light absorption by the superconductor would be a simple increase in the temperature of the superconducting film. If this was the only effect, then the photoresponse (change in the resistance of the superconducting line due to the light) would be proportional to dR/dT. This would then be a strictly bolometric effect. While the voltage photoresponse for some samples may be explained by the bulk, phonon heating of the superconducting film, others cannot be explained by such means[1,2]. Changes in

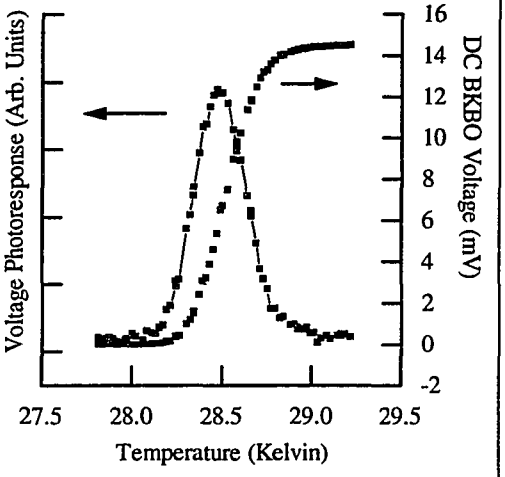

Fig. 1-1-1 Resistive Transition and Voltage Photoresponse of BKBO vs Temperature Showing Bolometric (dR/dT) Photoresponse

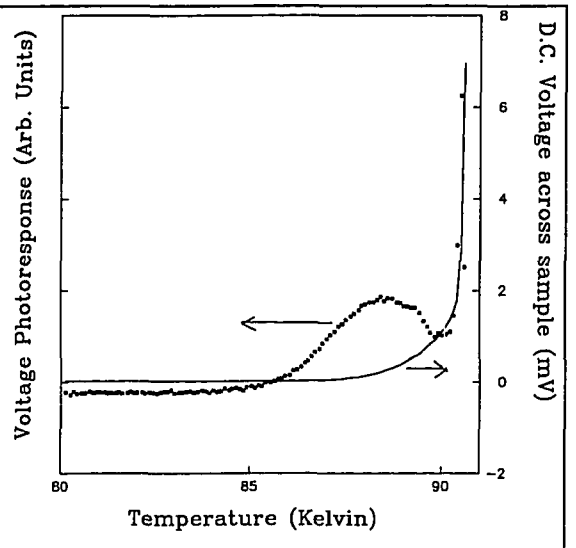

Fig. 1-1-2 Resistive Transition and Voltage Photoresponse of YBaCuO vs Temperature Showing Non-Bolometric Photoresponse

1 M. Leung, U. Strom, J. C. Culbertson, J.H. Claassen, S. A. Wolf, and R. W. Simon, Appl. Phys. Lett. **50**, 1691 (1987)

resistance due to the light that are not be proportional to dR/dT cannot be explained by a simple heating model and for the ease of terminology will be considered non-bolometric throughout this thesis. The photoelectric effect is an example of such an effect, although it clearly is not responsible for these voltages. An example of a bolometric voltage photoresponse is shown in figure 1-1-1 and an example of a nonbolometric voltage photoresponse is shown in figure 1-1-2. Some granular samples of Al, Sn, NbN and granular $YBa_2Cu_3O_{7-x}$ show a very large voltage photoresponse near the superconducting transition where the voltages are very large and have a rapid onset[3,4]. In these films it has been proposed that the voltages are caused by phase slips between the superconducting grains leading to vortex-induced voltages. Both bolometric[5,6,7,8,9] and nonbolometric photoresponse have also been seen in high temperature superconducting samples[10,11,12,13,14,15].

---

2 M.Lindgren, V. Trifonov, M. Zorin, M. Danerud, D. Winkler, B.S. Karasik, B.N. Gol'tsman, E.M. Gershenzon, Appl. Phys. Lett. **64**, 3036 (1994)

3 K. Weiser, U. Strom, S. A. Wolf, and D. U. Gubser, J. Appl. Phys. **52**, 4888 (1981)

4 J.C. Culbertson, U. Strom, S. A. Wolf, P. Skeath, E.J. West, and W.K. Burns, Phys. Rev. B **39**, 12359 (1989)

5 N. Fujimaki , Y. Okabe, and S. Okamura, J. Appl. Phys. **52**, 912 (1981)

6 G.L. Carr, M. Quijada, D.B. Tanner, C.J. Hirschmugl, G.P. Williams, S. Etemad, F. DeRosa, T. Venkatesan, B. Dutta, D. Hemmick, and X. Xia, SPIE **1292**, 187 (1990)

7 A.M. Kadin, W.R. Donaldson, J.H. Scofield, and L. Bajuk, SPIE **1292**, 176 (1990)

8 W.R. Donaldson, A.M. Kadin, P.H. Ballentine, and R. Sobolweski, Appl. Phys. Lett. **54**, 2470 (1989)

9 C.G. Levey, S. Etemad, and A. Inam, Appl. Phys. Lett. **60**, 126 (1992)

10 Keiichi Tanabe, Syugo Kubo, Youichi Enomoto, Hidefumi Asano, and Akihiko Yamaji, Jpn. J. of Appl. Phys. **30**, L110 (1990)

11 Mark Johnson, Appl. Phys. Lett. **59**, 1371 (1991)

12 R.S. Nebosis, M.A. Heusinger, W. Schatz, K.F. Renk, G.N. Gol'tsman,B.S. Karasik, A.D. Semenov, and G.M. Gershenzon, Optics Lett. **18**,96 (1993)

13 Gi. Schneider, P.G.Huggard, T. O'Brien, P. Lemoine, W. Blau, and W. Prettl, Appl. Phys. Lett. **60**, 648 (1992)

14 A.D. Semenov, G.N. Gol'tsman, I.G. Gogidze, A.V. Sergeev, P.T. Lang, K.F. Renk, Appl. Phys. Lett. **60**, 903 (1992)

The films that exhibit a non-bolometric effect are granular and show a photoinduced voltage at temperatures below the base of the superconducting transition. The major objective of this experiment is to investigate the mechanism producing these voltages. It has been proposed that these voltages may be created by vortex-antivortex pairs created (or depaired) by a short-lived local hot spot created by the absorption of a single photon[16,17,18]. The motion of these vortices as the applied current moves them across the superconducting line would then cause the observed voltages, and determining the presence or absence of these photon-induced vortex-antivortex pairs is the crux of the experiment[19,20]. A brief description of vortices, vortex-antivortex pairs and their depairing is given in chapter two.

2: Photon-Induced Vortex-Antivortex Pair Experiment

We have performed two specific experiments designed to determine the magnetic response of a current-carrying superconducting line with and without the presence of light. There are voltage measurements that support the photon-induced vortex-antivortex creation theory,[21] but they are not decisive and do not rule out the possibility that other mechanisms may create the observed voltages. Using a dc SQUID (Superconducting Quantum Interference Device) and the proper film geometry one can, in principle, detect a single

---

15 A. Kleinhammes, C.L. Chang, W.G. Moulton, and L.R. Testardi, Phys. Rev. B **44**, 2313 (1991)

16 A. M. Kadin, M. Leung and A. D. Smith, Phys. Rev. Lett. **65**, No. 25, 3193 (1990)

17 A.M. Kadin, M. Leung, A.D. Smith, and J. M. Murduck, Appl. Phys. Lett. **57**, 2847 (1990)

18 A.M. Kadin, J. Appl. Phys. **68**, 5741 (1990)

19 John Bardeen and M.J. Stephen, Phys. Rev. **140**, A1197 (1965)

20 Y. Avishi and Y.B. Band, Phys. Rev. Lett. **66**, 1761 (1991)

21 G. L. Garr, D. R. Karecki, and S. Perkowitz, J. Appl. Phys. **55**, 3894 (1984)

vortex-antivortex pair[22]. Since the depairing and subsequent motion of a single vortex-antivortex pair creates a voltage spike that integrated over time is no greater than $2x10^{-15}$ volt-seconds, a direct method for detecting the magnetic field from these vortices may prove more sensitive than a voltage measurement. The SQUID-based detection experiment also has the advantage that it can look for the magnetic signal of the vortices directly and not have to hypothesize their existence from the secondary voltage effect. Using a SQUID-based detector we have observed the magnetic signal from both thermally activated and photon-induced vortex-antivortex pairs. In this text, "photon-induced vortex-antivortex pairs" refers to both pairs created by the light and previously existing pairs which have been depaired by the light.

Two experimental approaches have been used to look for these photon-induced vortex-antivortex pairs. The first method involves using an applied current to drive the vortices toward one side of a superconducting line and antivortices toward the other. For a narrow line, one where vortices travel distances on the same scale as the line width before combining with antivortices and annihilating one another, the net flow of vortices out of any region is then approximately equal to the vortex generation rate, leading to a non-zero gradient across the line in the magnetic field due to the vortices. Changes in this field due to the light will be measured by the SQUID connected to a flux gradiometer[23]. As the line width and / or the vortex density grows, vortex-antivortex recombination will be an increasingly important factor. This will reduce the gradient across the line. A detailed calculation of the magnetic field gradient is contained in appendix C. The second method involves a ring-shaped sample that has an applied current running through it. If a vortex-

---

22 John Clarke, Wolfgang M. Goubau, and Mark B. Ketchen, J. Low Temp. Phys. **25**, 99 (1976)

23 K. Enpuku, R. Cantor, and H. Koch, J. Appl. Phys. **71**, 2338 (1992)

antivortex pair is depaired and the vortices are driven toward opposite sides of the line, the net flux through the ring is altered. This net flux is then measured by the dc SQUID.

The method which involves measuring the field gradient above the superconducting line has the advantage of being able to observe directly the magnetic field from the vortex-antivortex pairs and may be modeled for all resistance values, but its sensitivity is far less than that of the ring experiment. The ring experiment is difficult to model accurately for large vortex densities and does not measure the magnetic field from the vortex-antivortex pairs directly, but is far more sensitive than the gradiometer method.

The results of both methods have been compared to theories of uniform and non-uniform (local) heating of the superconductor by the photons. In the case of uniform heating of the superconductor, the magnetic photoresponse of the superconductor in the presence of light should be the same as without the light present, only with the temperature of the illuminated part of the sample shifted with respect to the temperature of the sample's surroundings. This gives a bolometric response. The data is also compared to that expected in the case of non-uniform heating of the superconductor, where the absorption of a photon creates a short-lived local depression of the superconducting electron density which leads to the creation of vortex- antivortex pairs at a rate linearly dependent on the power of the incident light irradiation.

Photon - induced vortex-antivortex pair breaking has the potential to be a useful detector mechanism, owing to the potential for high sensitivity and since the useful wavelengths would be tunable by adjusting the type of superconducting film (i.e., granular In-InO_x, Nb-Al arrays, $YBa_2Cu_3O_{7-x}$, etc.).

3: Kosterlitz - Thouless Experiment

The detection mechanisms described above are capable of detecting vortices which are thermally produced as well as those which are photo-induced. For this reason the presence or absence of thermally created vortex-antivortex pairs will also be noted. Thermally-activated vortex-antivortex pair creation has been extensively studied in two-dimensional superconducting films and Josephson-coupled superconductor arrays. In order to form free Kosterlitz-Thouless vortices over an observable temperature range the superconducting film must be thin compared to the magnetic penetration depth. All of the samples studied have this property with the exception of the $YBa_2Cu_3O_{7-x}$. A thick $YBa_2Cu_3O_{7-x}$ film would only be expected to produce free Kosterlitz-Thouless vortices over an observable temperature range if it behaved as a 2-d superconductor due to weak interplaner coupling[24,25,26]. In superconductors with weak interlayer coupling, vortex-antivortex pairs confined to a small number of layers could be created, independent of the thickness of the superconducting film. There is much evidence that the bismuth and thallium-based high temperature superconductors have very weak interplaner coupling and act as a stack of weakly linked very thin films[27]. This 2-d behavior has also been seen for oxygen deficient $YBa_2Cu_3O_{7-x}$[28] and for fully oxygenated $YBa_2Cu_3O_{7-x}$ at high current densities[29]. These films would then be able to produce K-T vortices and perhaps photon-induced vortices[30]. Since $YBa_2Cu_3O_{7-x}$ is known to have a magnetic screening length of

---

24 S.Q. Chen, W.J. Skocpol, E. DeObaldia, M. O'Malley, and P.M. Mankiewich, Phys. Rev. B **47**, 2936 (1993)

25 H.A. Blackstead, D.B. Pulling, and C.A. Clough, Phys Rev. B **44** (1991)

26 Petter Minnhagen and Peter Olsson, Phys Rev. B **44**, 4503 (1991)

27 S. N. Artemenko and Yu. I. Latyshev, Mod. Phys. Lett. B **6**, 367 (1992)

28 B. Janossy, D. Prost, S. Pekker and L. Fruchter, Physica C **181**, 51 (1991)

29 S. Q. Chen, W. J. Skocpol, E. DeObaladia, M. O'Malley, and P.M. Mankiewich, private communication

30 P. Minnhagen and P. Olsson, Physica Scripta **T42**, 29 (1992)

about 140 nm for a field directed perpendicular to the planes, a 2-d "pancake" vortex[31] in the middle of a thick (d ~ 200 nm) film could then be detected with a sufficiently coupled superconducting quantum interference device (SQUID). The detection of such vortices would then strongly support the theory of weak interlayer coupling. Such detection would also provide magnetic evidence for vortex-antivortex pairs that to date has existed only for the problematic situation of samples that have a temperature gradient across them[32,33,34,35].

Three different types of samples have been studied, Nb-Al arrays, In-InO_X films and $YBa_2Cu_3O_{7-X}$. The arrays were chosen because they form a good model system and they are well understood by several members of the group who could provide their expertise and well-characterized samples. The In-InO_X films were chosen as a well-known Kosterlitz-Thouless superconductor that was thought to be a promising candidate for photo-inducted vortex-antivortex pair creation. $YBa_2Cu_3O_{7-X}$ was chosen for several reasons. First and foremost, it is the best - characterized and developed of the high temperature superconductors. While $YBa_2Cu_3O_{7-X}$ is not the most two-dimensional of the high temperature superconductors, and therefore not the most likely to display photon-induced vortex-antivortex depairing, it is the most technologically interesting, so the decision was made to search for photon-induced vortex-antivortex depairing in this material. In addition, two sources of films - Laura Greene's group and my own production - were available.

---

31 John R. Clem, Physica A **200**, 118 (1993)
32 J.C. Garland, D.J. Van Harlingen, Phys. Rev. Lett. **55**, 2047 (1985)
33 Peter A. Bancel and K.E. Gray, Phys. Rev. Lett. **46**, 148 (1981)
34 Hu Jong Lee, D. A. Rudman, and J. C. Garland, Phys. Rev. Lett. **55**, 2051 (1985)
35 A.E. Koshelev, G. Yu Logvenov, V.A. Larkin, V.V. Ryazanov, and K. Ya. Soifer, Physica C **177**, 129 (1991)

II. THEORY

1: Vortex Theory / Kosterlitz-Thouless Theory

The experiments center on the detection of magnetic vortices in current-carrying superconductors. In order to understand the nature of vortices it is instructive to first look at how a superconductor interacts with a static homogeneous magnetic field.

First consider a superconducting sample in a very small magnetic field. Screening currents are established to expel the magnetic field from the interior of the sample. The length scale on which the field drops off is known as the magnetic penetration depth or the London penetration depth λ. The superconducting condensate may vary over distances longer than the Ginzburg-Landau coherence length ξ without undue energy increases. For superconductors with $\lambda/\xi < 1/\sqrt{2}$ the surface energy is positive[36] and the superconductor will continue to expel the magnetic field until the magnetic field energy becomes greater than the energy gained by forming the superconducting condensate, destroying the superconductivity of the sample and the screening currents along with it. Such superconductors are called type I superconductors.

For superconductors with $\lambda/\xi > 1/\sqrt{2}$ the surface energy is negative and this has a very large effect on the interaction of the superconductor with the magnetic field[37]. Such superconductors are known as type II superconductors. Below a lower critical field H_{c1} the magnetic field is completely expelled from the bulk of the superconductor. Between magnetic field strengths known as H_{c1} and H_{c2} the superconductor will divide itself into normal regions penetrated by the magnetic field and superconducting regions where the

---

36 M. Tinkham, Introduction to Superconductivity, Krieger Publishing Co. (1975)
37 A. A. Abrikosov, Soviet Phys. - JETP **5**, 1174 (1957)

field is expelled. The process of dividing the superconductor into these regions will seek to maximize the interface area. The tubes of magnetic flux create normal regions and form the core of the magnetic vortices. There are two limitations on this process of division: the coherence length ξ and the fact that each vortex must contain at least a certain minimum quantity of magnetic flux[38]. The coherence length limits the density of magnetic vortices near H_{c2}, where $\xi^2 \approx \Phi_0/B$ and the cores are nearly overlapping. Flux quantization limits the vortex density to the density of vortices needed to equal the externally applied flux.

The lower limit of the flux contained by a vortex is set by the condition that the wavefunction of the superconducting condensate must be single valued, so that the phase drop around any closed loop must be an integer multiple of 2π. Since a phase drop of zero around a closed loop will lead to no net current flow (for an s-wave superconductor in the absence of a field) and therefore no flux enclosed, the smallest non zero amount of flux possible in a vortex corresponds to a phase drop of 2π around the vortex. The resulting flux in a single vortex works out to $2.07 \cdot 10^{-15}$ Wb. The energy required to create a vortex with a phase drop of 4π or greater is large enough that for the purposes of this work when a vortex is referred to it implies a vortex with a phase drop of 2π.

Above H_{c2} the energy density of the magnetic field is greater than the energy density of the superconducting condensate so the superconductivity is destroyed and the field penetrates the sample fully. All of the superconducting samples studied in this work are firmly in the type II regime.

A vortex may also exist in the absence of an externally applied magnetic field. Perhaps the most common example of this is the thermal generation of vortex-antivortex pairs that form in thin superconducting films. Here an antivortex is identical to a vortex

---

38 Tinkham, Introduction to Superconductivity, Krieger Publishing Co. p. 151 (1975)

but with an opposite sign on the phase drop, -2π instead of 2π. This leads to a magnetic field in the opposite direction from that of a vortex. Since the "positive direction" and the "negative direction" for phase drops are arbitrarily defined, the designation of which vortices are referred to as "vortices" and which are referred to as "antivortices" is also arbitrary.

The free energy per unit length of a vortex-antivortex pair is given as

$\Delta F = 2\left[\frac{\Phi_o}{8\pi}h(\vec{r}_1)\right] + \frac{\Phi_o}{4\pi}h(\vec{r}_2)$ where $h(\vec{r}) \approx \frac{\Phi_o}{2\pi\lambda^2}\left[\ln\frac{\lambda}{r} + 0.12\right]$ for $\zeta \ll r \ll \lambda$ and

$h(r) \rightarrow \frac{\Phi_o}{2\pi\lambda^2}\left(\frac{\pi\lambda}{2r}\right)^{1/2} e^{-r/\lambda}$ for $r \rightarrow \infty$, where ζ is the Ginzburg-Landau coherence length and λ is the 2-d magnetic penetration length[39]. As the vortices become close on the scale of the magnetic penetration length, the currents generated by the vortices begin to overlap, creating an attractive force. When the vortex and antivortex are located in the same place (zero separation) this overlap of currents and their associated magnetic fields causes complete cancellation and there is no net current or field. At this point the energy associated with the vortex-antivortex pair is zero and the vortex-antivortex pair has for all practical purposes ceased to exist. For this reason vortex-antivortex pairs with separations small compared to the penetration depth λ require very little energy to form and are thermally created very easily. However, these vortex-antivortex pairs are strongly bound and therefore do not contribute any resistivity to the superconductor except in the presence of a very large current density. They also will quickly recombine.

As the temperature is increased vortex-antivortex pairs are formed with increasing separation between the vortex and the antivortex. At sufficiently high current densities the attractive force between the vortex and antivortex may be overcome by a force of separation due to the applied current exerting forces in opposite directions on the vortex

---

39 Tinkham, Introduction to Superconductivity, Krieger Publishing Co. p. 149 (1975)

and antivortex. Vortex pairs which are depaired in this manner will cause a voltage to appear as they are moved across the superconductor.

In addition to an isolated vortex-antivortex pair causing a voltage to appear across a superconducting line as they are separated by a large current density, a large number of vortex-antivortex pairs may have a collective effect whereby any applied current density will give rise to a voltage across the superconductor[40,41]. This occurs when the separation between the vortex and antivortex of an individual pair is large compared to the distance between the centers of adjacent vortex-antivortex pairs. In this situation the attractive force between the vortex and the antivortex in a vortex-antivortex pair is screened out by the large number of other vortices between them. The vortices will then act as unpaired vortices and create a voltage across the superconductor in the presence of any non zero current density. The resistance per square is given by $2\pi R^n n_f \zeta^2(T)$ where R^n is the normal state resistance, n_f is the vortex density and $\zeta(T)$ is the Ginzburg-Landau coherence length[42]. The resistance in this regime is ohmic. As the temperature is lowered, eventually a critical temperature, T_{KT}, is reached where the vortex density and average vortex-antivortex pair separation have decreased so that the screening effect is no longer sufficient to depair vortices and the superconductor enters into a zero resistivity state for low current densities. As the current density is increased, a non zero resistance is observed which is nonlinear in applied current density. This critical temperature is known as the Kosterlitz-Thouless temperature. Superconducting films that display this effect are known as Kosterlitz-Thouless (K-T) superconductors. These films, in the limit of an infinite system, lose all resistivity below the Kosterlitz-Thouless unbinding temperature T_{KT}, where the free vortices become bound.

---

40 J. M. Kosterlitz and D. J. Thouless, J. Phys. C **6**,1181 (1973)

41 A.N. Samus, A.F. Popkov, V.I. Makhov, I.B. Krynetskii, I.V. Zolotukhin, and A.K. Zevezdin, Superconductivity **4**, 1229 (1991)

42 B. I. Halperin and David R. Nelson, J. Low Temp. Phys. Vol. **36**, 599 (1979)

2: Photon-Induced Vortex-Antivortex Pair Creation Theory

As briefly mentioned in chapter 1, it has been proposed that the nonbolometric voltage photoresponse of some granular superconductors may be caused by photoinduced vortex-antivortex pairs which are depaired by the applied current. Kadin et al[43] have proposed a mechanism in which the absorption of a single photon by the superconducting condensate creates a short lived electronic hot spot where the electronic temperature locally is significantly higher than the local phonon temperature[44,45]. This will cause a depression in the critical current at that spot. It should be noted that such a spot can only be formed by a single photon or a group of photons all absorbed at the same location and at the same time. If the sample is biased at a sufficiently high current density, the current will distort as it flows by this point. The current pattern formed by such a distortion is very similar to that formed by a vortex-antivortex pair centered on that spot having a separation of the order of the spot size. Such a current distortion, in the presence of an applied current, may form a vortex-antivortex pair which can be pulled apart by the applied current, causing the observed voltage. A vortex-antivortex pair depaired in this manner will be referred to as a photon-induced vortex-antivortex pair. The bulk heating of the superconductor due to the absorbed photons could also enhance the number of pairs thermally depaired, and they could also be considered photon-induced vortex-antivortex pairs, but for clarity in my terminology vortex-antivortex pairs that are depaired by a thermal shift caused by the bulk heating of the sample by the accumulation of absorbed photons will not be included in the definition of the term photon-induced vortex-antivortex pairs.

---

43 Y. Cai, P.L. Leath, and Z. Yu, Phys. Rev. B **49**, 4015 (1994)
44 A. M. Kadin, M. Leung and A. D. Smith, Phys. Rev. Lett. **65**, 3193 (1990)
45 P.L. Leath and W. Xia, Phys. Rev. B **44**, 9619 (1991)

While this effect may in theory occur in reasonably thick (~1000 - 2000 Angstroms) films, photons of the wavelength used to observe the unusual voltages described earlier are unable to create a local electronic hot spot large enough to form a vortex-antivortex pair with sufficient separation that the applied current could depair them. It is far more likely that a photon which is absorbed in an already existing weak link may suppress the critical current of that weak link enough to depair a preexisting vortex-antivortex pair. It is also conceivable that a photon-induced vortex-antivortex pair may be created in a very thin homogeneous film. Such an experiment on a very thin film is attempted using oxygen reduced $YBa_2Cu_3O_{7-x}$ to simulate a stack of independent thin films.

3: Summary of the Magnetic Field Calculation

While the expected signal will be different for the two experimental approaches, the basic physics that must be understood is the same. The two basic physical phenomena that must be understood are as follows:

The spatial dependence of the current density (and the magnetic field associated with it) will vary as the temperature is varied in the absence of any magnetic vortices. The current shifts toward the edges of the current carrying line as the temperature is decreased[46]. This will cause a change in the magnetic field over the line and should be kept in mind in order to have a complete understanding of the physics of the experimental setup.

How a system of vortex-antivortex pairs being generated at a certain rate will interact with an applied current and with itself, and the resulting vortex dynamics, must also be understood. In this section an outline of the calculation is presented. Readers interested in more mathematical rigor should consult appendix A.

---

46 E.H. Rhoderick, Nature **194**, 1167 (1962)

A component of the magnetic field due to the presence of free vortices can arise in the presence of a transport current. This may both create a gradient across the line, which is measured in the gradiometer experiments to be described later, and may change the total flux through the loop in the loop experiments by a flow of vortices out the edges of the film. For this calculation the vortex creation rate is held constant across the line, unlike the case of when there is a temperature gradient.

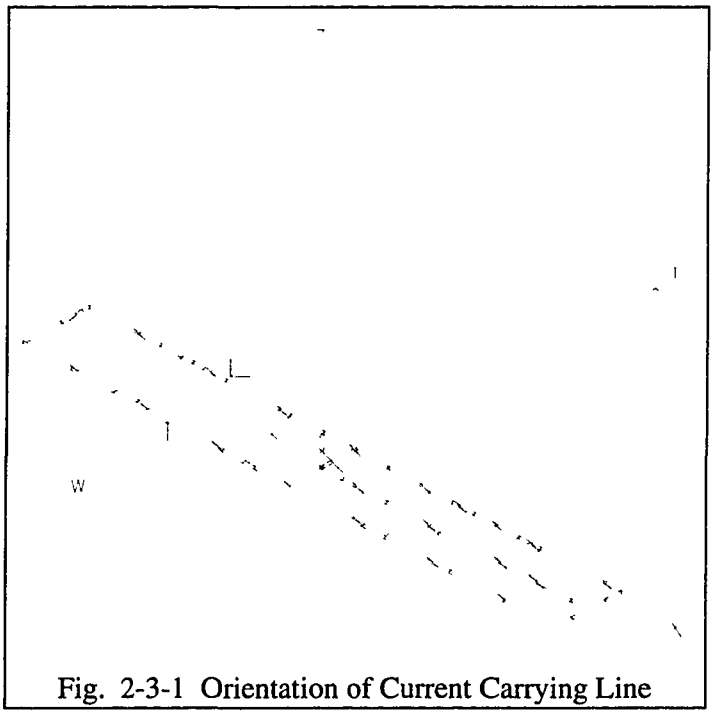

Fig. 2-3-1 Orientation of Current Carrying Line

The symbols used in the vortex flux calculation are:

B = field due to vortices $n^{\pm} = \pm$ vortices/m^2

$G^{\pm} = \pm$ Vortex creation rate kn^+n^- = Vortex recombination rate

$v\partial_x n^{\pm}$ = Net ± vortex flow out of region

The steady state equation of continuity is: $v\partial_x n^+ = G - kn^+n^-$; $v\partial_x n^- = -G + kn^+n^-$. The resulting differential equation for the density of vortices is nonlinear and behaves quite differently in different regimes of vortex density and experimentally controlled parameters. While a complete tackling of the entire beast is in appendix A, for the ease of understanding a qualitative look at several cases follows.

Case #1: An infinite film with a spatially uniform creation rate

In this, the simplest case, in any region the vortices are created and recombined at the same rate. When this occurs there is no net flow of vortices into or out of the region, so the vortex density will adjust so that the vortex recombination rate equals the vortex generation rate. In this simple case the gradient in the magnetic field due to the vortices is always zero.

Case #2: A wide film with a spatially uniform creation rate

For a wide line, whose width is large compared to the average distance that a vortex travels before recombining with a antivortex, the net flow of vortices out of the line through the edges will be very small compared to the vortex recombination rate and may then be ignored. The system would then behave like the simple case described above except near the edges of the line. Near these edges, the vortices begin to behave like those described in case #3 for a narrow line.

Case #3: A narrow film with a spatially uniform creation rate

For a narrow line, whose width is small compared to the average distance that a vortex travels before recombining with an antivortex, the rate of vortices flowing out of the line through the edges is much larger than the vortex recombination rate. In this limiting case vortex recombination plays a very small role in the vortex dynamics and may then be ignored. The net flow out of the region is then approximately equal to the vortex generation rate. The steady state equation of continuity for the region of interest becomes

$\partial_x n^+ = \frac{G}{v} \quad \partial_x n^- = -\frac{G}{v}$. This leaves $n^+ = a_o + a_1 \frac{x}{w} \qquad n^- = a_o - a_1 \frac{x}{w}$.

In this case there would be a non-zero gradient in the magnetic field across the entire line due to the vortices and a net flow of vortices across the line, changing the net flux through the loop in the loop experiments.

Case #4: A film with vortex creation confined to a spot in the interior of the film

In this case the vortices may recombine while they are within the spot where they are being created. Once they are driven out of this spot, no further recombination may occur. This is due to the fact that only vortices will be driven to one side and only antivortices will be driven to the other, leaving nothing to recombine with. A magnetic field will be generated by the flow of vortices out one side of the spot and a oppositely directed magnetic field will be generated by the antivortices driven out the other side of the spot.

As mentioned earlier, a general solution to the vortex density problem for all vortex densities and line widths is presented in appendix A, Magnetic Field Calculation.

In order to detect vortex-antivortex pairs free vortices must be able to travel distances on the same scale as the line width without combining with free anti-vortices and annihilating one another. This would require a mean free path of at least the order of microns in the presence of an imbalance in the number of vortices and antivortices large enough to create a detectable magnetic field for the gradiometer experiment to be successful. Since in the ring experiment the flux measured is that inside the ring, which is affected by any flux motion, the mean free path need not be comparable to the line width in order for the vortices to be detected.

Now the crucial question remains, when is the mean free path comparable to the line width? The vortex mean free path b is approximately[47] $b \cong \sqrt{\frac{1}{8\pi n_f}}$, where n_f is the density of free vortices, both thermally generated and photon induced. A mean free path of 10 μm would be obtained with a vortex density of 4×10^6 vortices/m^2. A detectable field of 10^{-8}T would then be obtained if an imbalance in the density of vortices to the density of antivortices of 1.2% were obtained. While this calculation is very encouraging,

---

47 Peter A. Bancel and K. E. Gray, Phys. Rev. Lett. **46**, 148 (1981)

since the equation for the mean free path of vortices was developed for homogeneous superconducting films it is not valid for the array data.

In the limit of the recombination rate being small, as in case #3, the field due to the vortices is $B = \Phi(n^+ - n^-) = \frac{2G}{v}x$.

Taking the temperature dependence for thermally generated free vortex-antivortex pairs at $G \propto \left(1-\left(\frac{T}{T_c}\right)^4\right)\sinh\left(\frac{5(T_{KT}-T_c)}{T-T_{KT}}\right)$, K-T vortices should create a field gradient

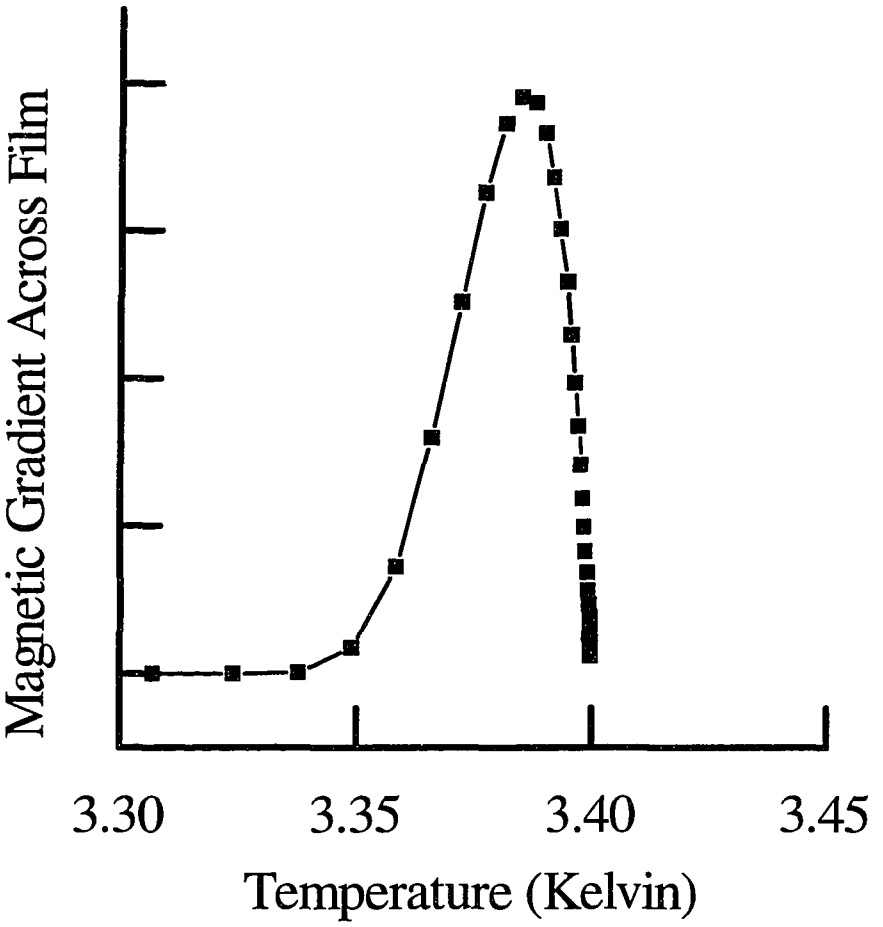

Fig. 2-3-2 Magnetic Response Due to Thermally Induced Vortices, Calculated using the T_{KT} of In-InO_X

across the film between T_c and T_{co}, superimposing a 'dip' in the field gradient across the film vs temperature due to current alone[48]. For comparison to the data taken on In-InO_x, the field due to vortices as a function of temperature is graphed in figure 2-3-2 using the T_c and T_{KT} of a In-InO_x sample.

48 J.C. Garland, D.J. VanHarlingen, Phys. Rev. Lett. **55**, 2047 (1985)

III. EXPERIMENTAL APPROACH

1: Physical Setup

The experiments were carried out in an insert which was cooled in a super-insulated dewar. The dewar is located in a screen room to reduce the radio frequency electrical noise. The data collecting computer and most of the electronics were located outside of the screenroom, with only the preamplifiers and the low-noise current supplies located inside the screenroom, as shown in figure 3-1.

The insert was built of several removable modules. The top of the insert consisted

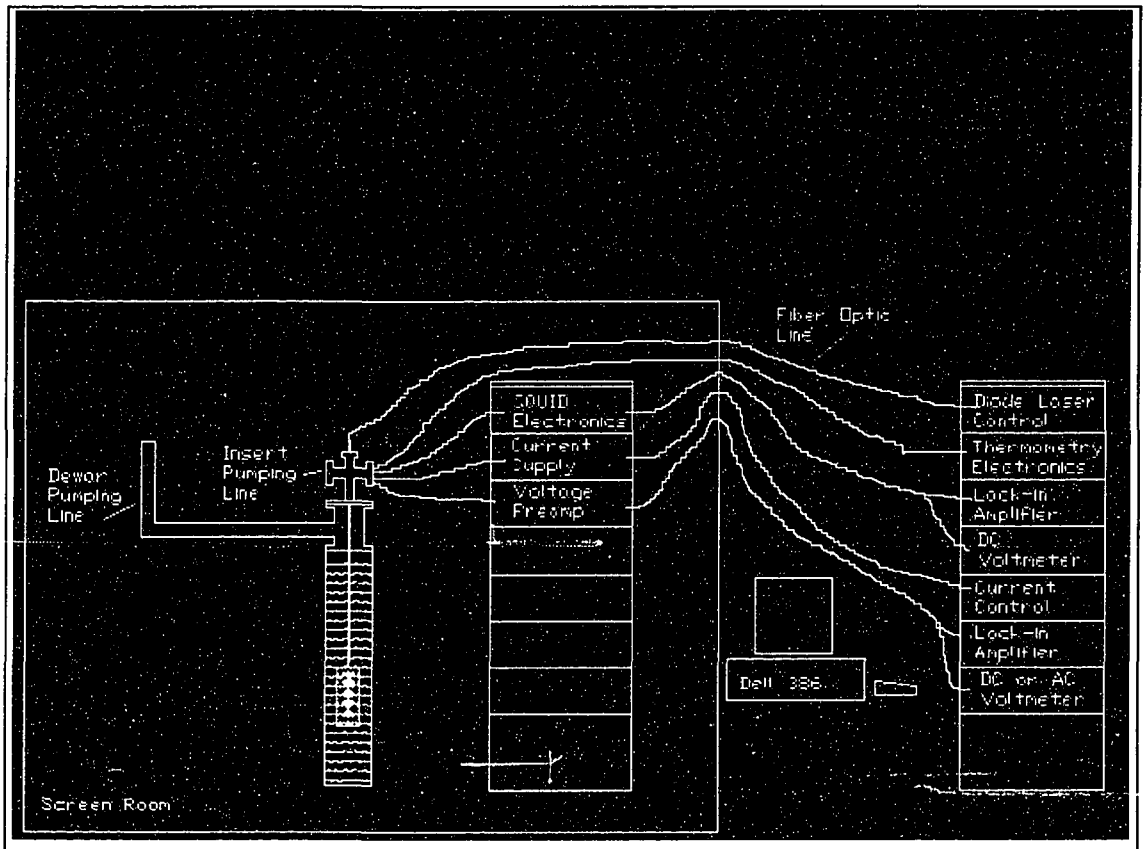

Fig. 3-1 Experimental Environment

of a six way cross with 2 3/4" conflat fittings at each end. This allows the use of commonly available components such as the gas handling and vacuum measurement devices used. It also allows the use of conflat blanks to create custom made but easily installed and removed components. The price of these fittings are comparable to standard o-ring based systems but provide greater strength and lower leak rates. One of these fittings was connected to the 3/4" tube going down to the vacuum can at the cold end of the insert. The other five fittings held feedthroughs for the electrical leads, fiber optic cable, vacuum pumping lines, gas backfill lines, pressure gauges and a pressure relief valve. The cold end of the insert, which was immersed in liquid helium, held a vacuum can with an indium o-ring seal. The top of this can, which was silver soldered to the 3/4" stainless steel tube, was tapped on the inside portion to hold the experimental apparatus, which can be changed readily to adapt to the various experiments.

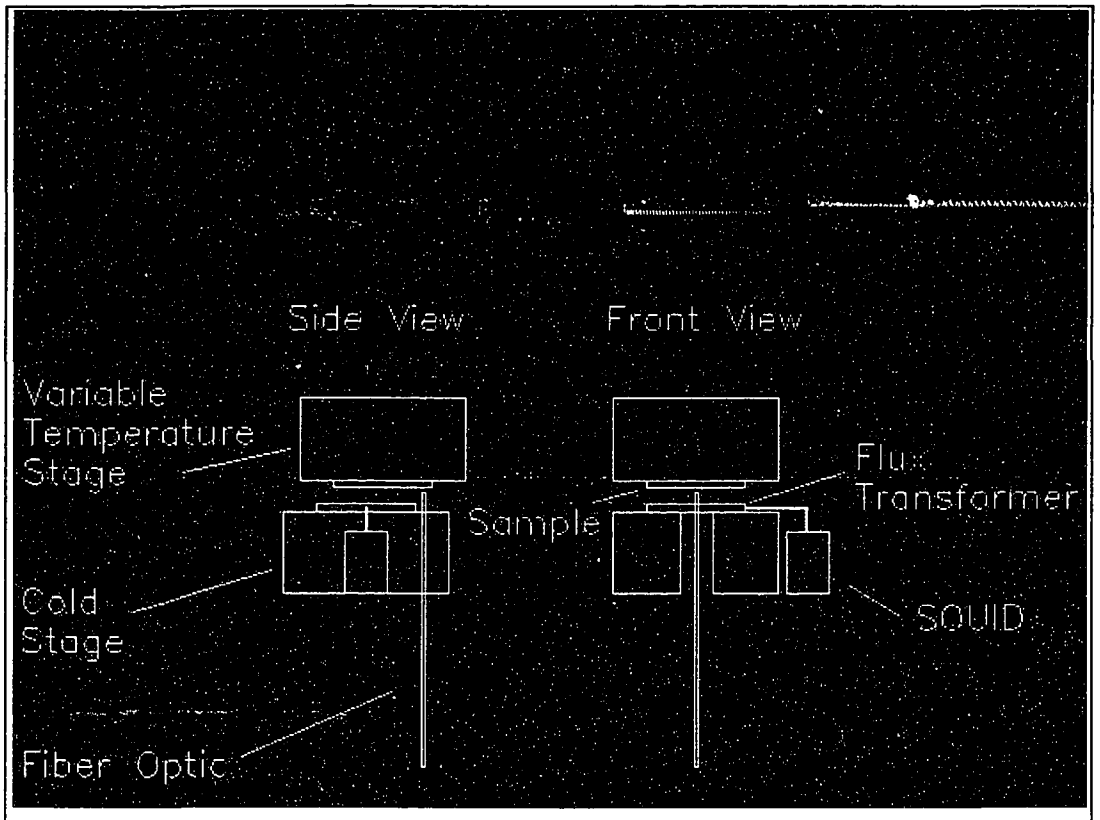

Fig. 3-2 Insert Schematic

The sample and detectors were located in a vacuum can at the bottom of the insert. This vacuum can was kept immersed in liquid helium which could be pumped on to provide cooling down to 1.4 K. The insert was evacuated before cooling down and any residual gases other than helium were cryropumped by the cold walls of the vacuum can. The residual helium pressure is then far too low to cause any appreciable cooling of the sample. The SQUID and sample were both cooled by thermal conduction to the walls of the vacuum can, which were in contact with the liquid helium. The SQUID and flux transformer were kept in strong thermal contact with the vacuum can and the sample was kept in very weak thermal contact, allowing the sample temperature to be varied without varying the SQUID's or the flux transformer's temperature appreciably. The sample was then positioned very close to, but not touching, the flux transformer to provide the needed magnetic coupling. Typical separations were 1 - 300 μm, which varied with the size of the flux transformer and were kept small compared to the size of the flux transformer.

The expected magnetic field strength may be determined from the photoresponse resistance data and an estimate of vortex velocity. For a voltage V arising from flux flow, $V = \frac{d\Phi}{dt} = \Phi_o \times n \times \frac{v}{w}$, where Φ_o is the flux of a single vortex, n is the number of vortices, v is the average vortex velocity and w is the sample width. This estimate assumes that the vortex mean free path is comparable to or larger than the line width. Signal size estimates are very rough due to the obvious variability of V/w for different currents, temperatures, photon absorption rates and materials. The flux flow resistance data in the literature gives voltages at 10^{-1}-10^{-5} V per meter and vortex velocities[27] should be in the range of 10^4 to 10^5m/s, giving fields in the range of 10^{-5} to 10^{-10} T.

Fields this small rule out the use of magnetic field detectors such as Hall probes, scanning tunneling microscopy (STM) and magnetic force microscopy (MFM)[49]. For this

---

49 Private communication, L. N. Vu and D.J. VanHarlingen

reason a Superconducting Quantum Interference Device (SQUID) was used as the main detector. The sensitivity of various magnetic field detection mechanisms is shown to the right in figure 3-3, with the sensitivity of the dc SQUID setup that I used given by the region marked SSM.

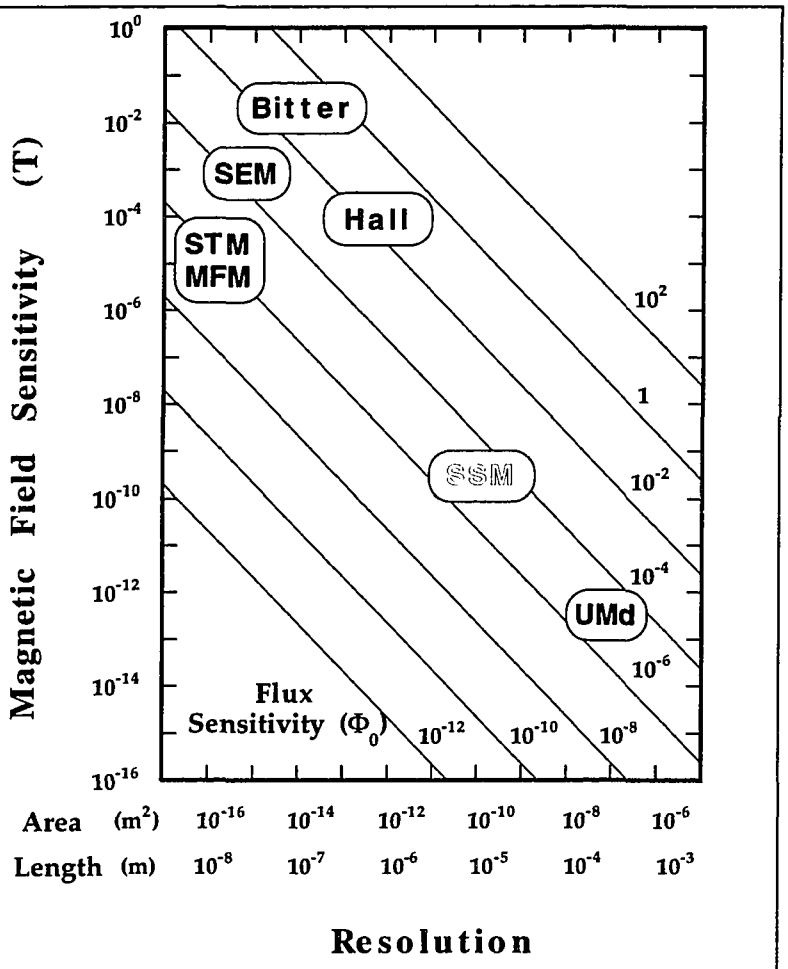

Fig. 3-3 A Comparison of Several Magnetic Field Detection Mechanisms

IV. EXPERIMENTAL DATA ON ARRAYS

1: Film Growth And Properties

The array was a 500×500 Al-Nb proximity-coupled superconducting array deposited in a cryropumped high vacuum chamber and patterned using standard photolithographic techniques. The cells consisted of Nb crosses, 1200 Å thick with line widths of 2 μm and a center to center distance of 20 μm. These cells were deposited on a layer of sputtered Al, approximately 1000 Å thick, which provided the cell to cell coupling. The gap width between adjacent cells was 1.2 μm. Figure 4-1-1 shows a similiar array, one of only 9x9 cells so that the individual cells may be seen. The black crosses are the niobium islands.

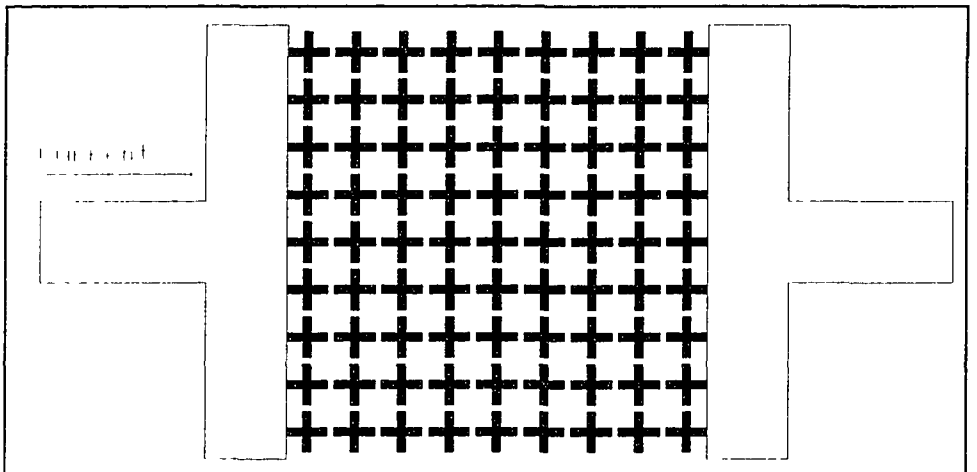

Fig. 4-1-1 Resistive Transition of the Array

The array was characterized by Subashri Rao using a rf-SQUID based voltmeter and it has been established that the array exhibits Kosterlitz-Thouless behavior near the superconducting transition[50,51]. The resistive transition of the array is shown in figure 4-1-

50 D.J. Resnick, J.C. Garland, J.T. Boyd, S. Shoemaker, and R.S. Newrock, Phys. Rev. Lett. **47**, 1542 (1981)

2. The sharp drop in resistance visible in the smaller inset graph, which covers the temperature range to above 200 K, is caused by the superconducting transition of the Nb islands at 9 K. The smoother drop in resistivity that begins around 4.8 K is due to the superconducting islands beginning to couple. This occurs when the coherence length of the superconducting electrons in the normal metal becomes long enough to allow a supercurrent to flow from one Nb island to the next. The Kosterlitz-Thouless transition is shown in the larger graph, and begins around 4.8 K when the Nb islands begin to couple to one another. The base of the Kosterlitz-Thouless transition (T_{KT}) occurs at around 3.5 K. The screening capability of the array is very small at magnetic fields of the order of one flux quantum per cell of the array.

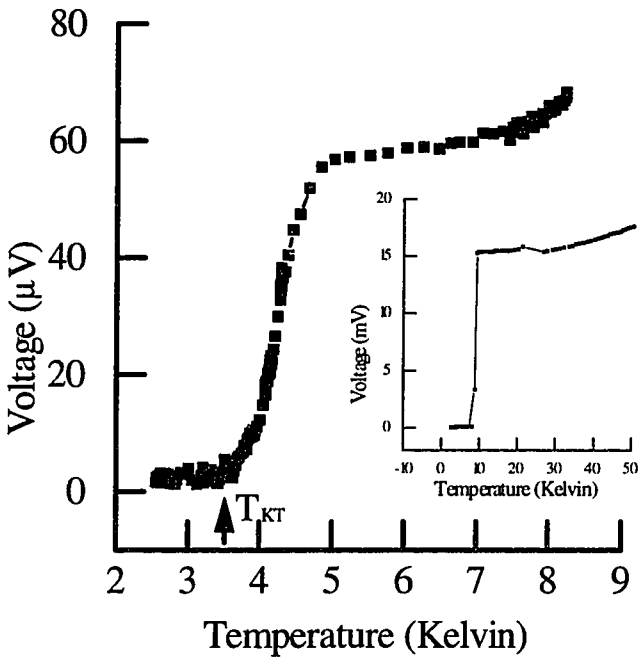

Fig. 4-1-2 Resistive Transition of the Array

51 B.J. Van Wees, Phys. Rev. B **44**, 2264 (1991)

2: Experimental Setup

The magnetic flux generated by the array was coupled to a dc SQUID using a flux transformer. The flux transformer was configured as a gradiometer centered over the array, so the flux transferred to the SQUID represents the gradient in the magnetic field over the array. The array was one centimeter on each side. The gradiometer was ~ 7 mm wide by ~8 mm long and centered over the array within ±1/2 mm. The gradiometer was thermally isolated from the array and was 100 - 500 μm above the array.

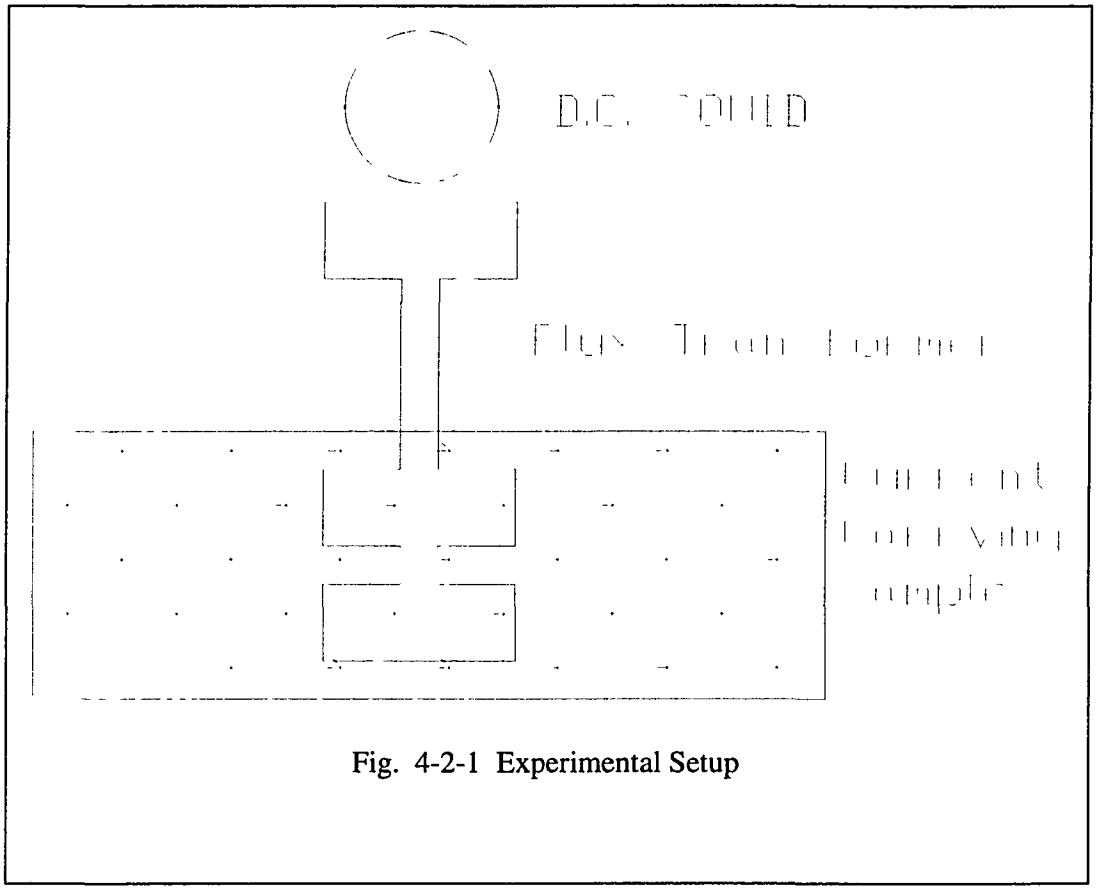

Fig. 4-2-1 Experimental Setup

Once created, a vortex-antivortex pair is detected by separating the vortex from the antivortex using an applied current, causing the positive polarity vortices to move toward one side of the array and the negative polarity vortices to move toward the other. The

resulting gradient in the magnetic field across the array, as measured by the SQUID, is the signal of interest. When optimized the SQUID has a resolution better than $10^{-5}\ \Phi_0 / \sqrt{Hz}$, which is sufficient to detect a low density of vortices passing under the flux transformer.

In the absence of a current, there should be no net field normal to the surface of the superconducting line. This can be shown by a simple symmetry argument. In the presence of a current, a gradient in the field across the line is not ruled out by symmetry and is expected due to the finite width of the sample and current redistribution. Furthermore, if photon induced vortex pairs are created and pulled apart by the current in the line then a gradient in the magnetic field perpendicular the film will be produced (see appendix A, Magnetic Field Calculation). Changes in this field due to the light will be measured by a SQUID. The signal from the sample to be picked up by the flux transformer can be thought of as twice the net density of vortices ($n^+ - n^-$) under one side of the detector times the area of one side of the detector. This is both a time and aerially averaged signal. The results will then be compared to the theories of uniform and non-uniform (local) heating of the superconductor by the photons.

3: Kosterlitz - Thouless Data

An array may be thought of as a model of a much smaller section of a granular film. Since the Nb islands of the array are physically much larger than the grains of the In-InO_X films and have a magnetic field which falls off only over a very long distance, the recombination cross section of magnetic vortices in an array is very large compared to a In-InO_X film. The transverse penetration depth ~100 μm. This is still small compared to the array, which is 1000 μm on a side, but gives a very large cross section for vortex-antivortex recombination. As a result, the average distance that vortices in the array are able to travel before recombining does not grow large enough for the vortices to be detected by the

gradiometer until the vortex density is very low, namely near T_{KT}. For this reason, no appreciable signal from thermally generated vortex-antivortex pairs may be seen except near T_{KT} in the array samples but an appreciable signal from the In-InO_x films is possible, as will be discussed in the next chapter. For this reason, no further analysis of the array data is attempted for the temperature region significantly above T_{KT}.

4: Photon - Induced Vortex - Antivortex Pair Data

Next the vortex signal due to photon-induced vortex-antivortex pairs is considered. Photon induced vortex measurements were made by pulsing the light onto the sample in the presence of a dc transport current. The flux through the SQUID was then measured using a lock-in amplifier tuned to the same frequency as the pulsed light. The light was pulsed at 30 - 2,000 Hz with a 50% duty cycle. These pulse lengths are very long with respect to all of the time constants of the photon absorption, electron - phonon relaxation and vortex motion. The data taken is then essentially a steady - state measurement. The ac flux through the SQUID due to the pulsed light is shown in

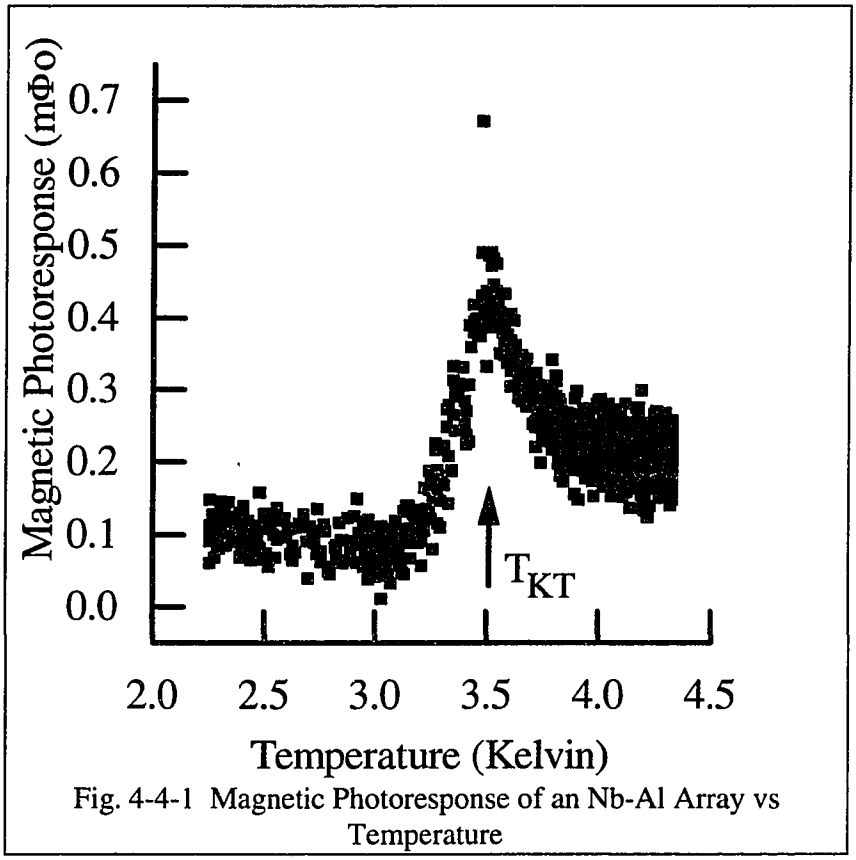

Fig. 4-4-1 Magnetic Photoresponse of an Nb-Al Array vs Temperature

figure 4-4-1 for an Nb-Al array. The photon-induced vortex component of the field is greatly reduced as the temperature falls below T_{KT} due to the large increase in energy required to form a free vortex-antivortex pair at these temperatures. The easiest (and hence most likely) way for a single photon to yield depaired vortices is for it to cause a previously existing pair to be depaired[52]. The thermal creation rate for these vortices is exponential in temperature[53], consistent with the photoresponse data shown here. Substantially above T_{KT} the increase in thermally-created vortices in the film prohibits the photon-induced vortex-antivortex pairs from separating enough to be detected before they recombine with other free vortices. The photon-induced vortex signal would then be concentrated at the Kosterlitz-Thouless transition temperature. This is precisely where the photoinduced signal peaks, so the temperature dependence of the signal is in good qualitative agreement with the expected result for photon-induced vortex-antivortex pairs, that being a signal that is exponentially decreasing below T_{KT} and falls off sharply above T_{KT}. Thermally created vortex-antivortex pair would, however, show a similar peak in the magnetic photoresponse at T_{KT}, so the challenge becomes determining whether this peak is due to thermally or photoinduced vortex-antivortex pair breaking. The most straightforward method would be to compare the magnetic photoresponse to the magnetic signal from the current without light being present to see if the magnetic photoresponse follows the bolometric form of being proportional to the slope of the magnetic photoresponse due to the current alone. Figure 4-4-2 shows the magnetic response to the current alone for the temperature range of interest. This data shows no sharp feature at T_{KT} at all, so the magnetic photoresponse data cannot be interpereted as a bolometric response based on the current path changing with temperature. In addition, the data is not of the form expected

---

52 M.B. Cohn, M.S. Rzchowski, S.P. Benz, and C.J. Lobb, Phys. Rev. B **43**, 12823 (1991)

53 B. I. Halperin and David R. Nelson, J. of Low Temp. Phys. **36**, 599 (1979)

for a bulk heating effect that merely changes the current distribution in the film due to the tendency for the current to pile up at the sides of the film as the sample attempts to screen out the magnetic field produced by the applied current. This can be deduced from the magnetic properties of the film vs temperature. It is expected that the temperature dependence of the screening of an externally applied magnetic field would have the same temperature dependence of the screening of the self-field. The screening of an external field vs temperature is shown in figure 4-4-3 and shows no sharp feature at T_{KT} that could account for the peak in the magnetic photoresponse. The screening capibility graph indicates the fraction of the magnetic flux that passes through the film as a function of temperature. The screening effectiveness was measured using a magnetometer where a current carrying wire was placed along the center of the gradiometer. The magnetic field from this wire induced a flux in the gradiometer and was then detected by the SQUID, as shown in figure 4-4-4. The magnetic flux measured by the SQUID was reduced at temperatures below Tc as the array began to magnetically shield the gradiometer from the applied flux.

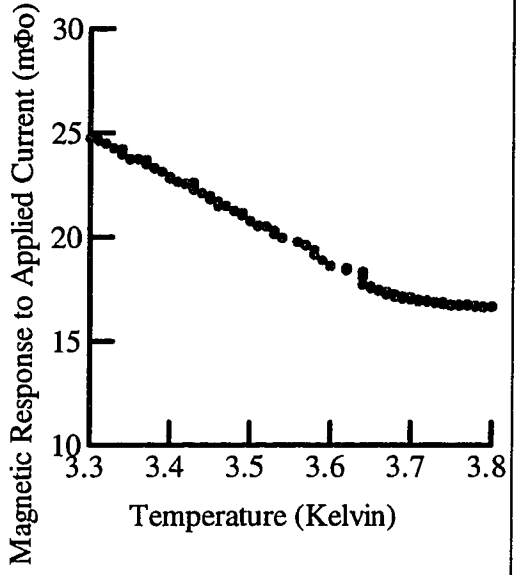

Fig. 4-4-2 Magnetic Response to an Applied Current Data vs Temperature on Nb-Al Array

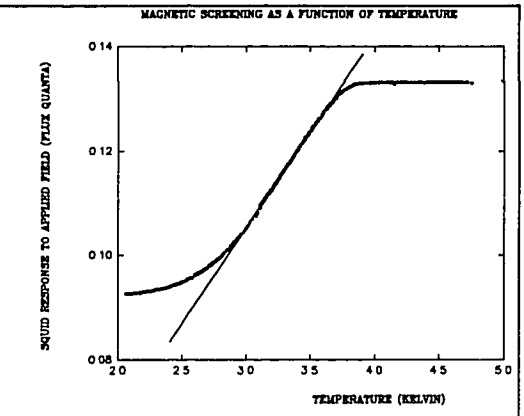

Fig. 4-4-3 Magnetic Screening Effectiveness vs Temperature on Nb-Al Array

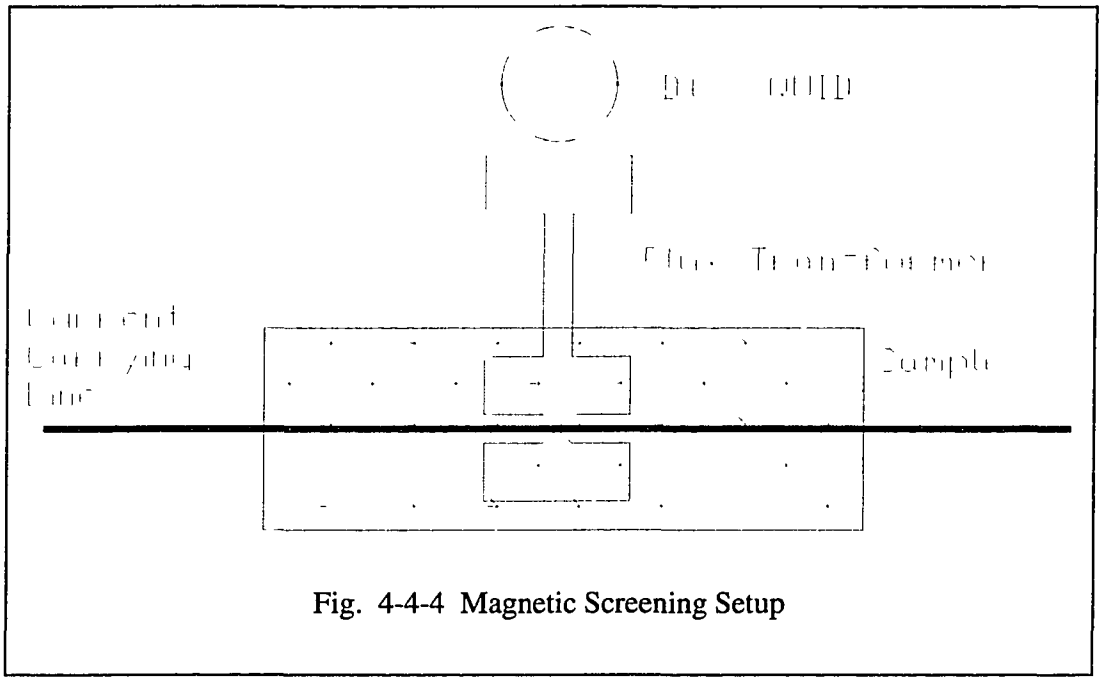

Fig. 4-4-4 Magnetic Screening Setup

Additional evidence, and perhaps the most convincing, that the photon-induced flux measured is from a photon-induced vortex-antivortex pair creation (or depairing) comes from the photon-induced flux vs. laser intensity data shown in figure 4-4-5. While the photoresponse vs temperature data has a functional form with many free parameters, which makes modeling of it easy but not overly instructive, the photoresponse vs intensity data to be considered next has a linear functional form with one fixed parameter (the intercept) and one free parameter (the slope). Although the bulk heating of the sample due to the light is proportional to the laser intensity, neither the current distortion nor thermally activated vortex-antivortex density are expected to scale linearly with temperature. As shown in figure 4-4-5, the measured ac flux signal through the SQUID is linear in laser intensity (at the sample) as would be expected for a single photon effect.

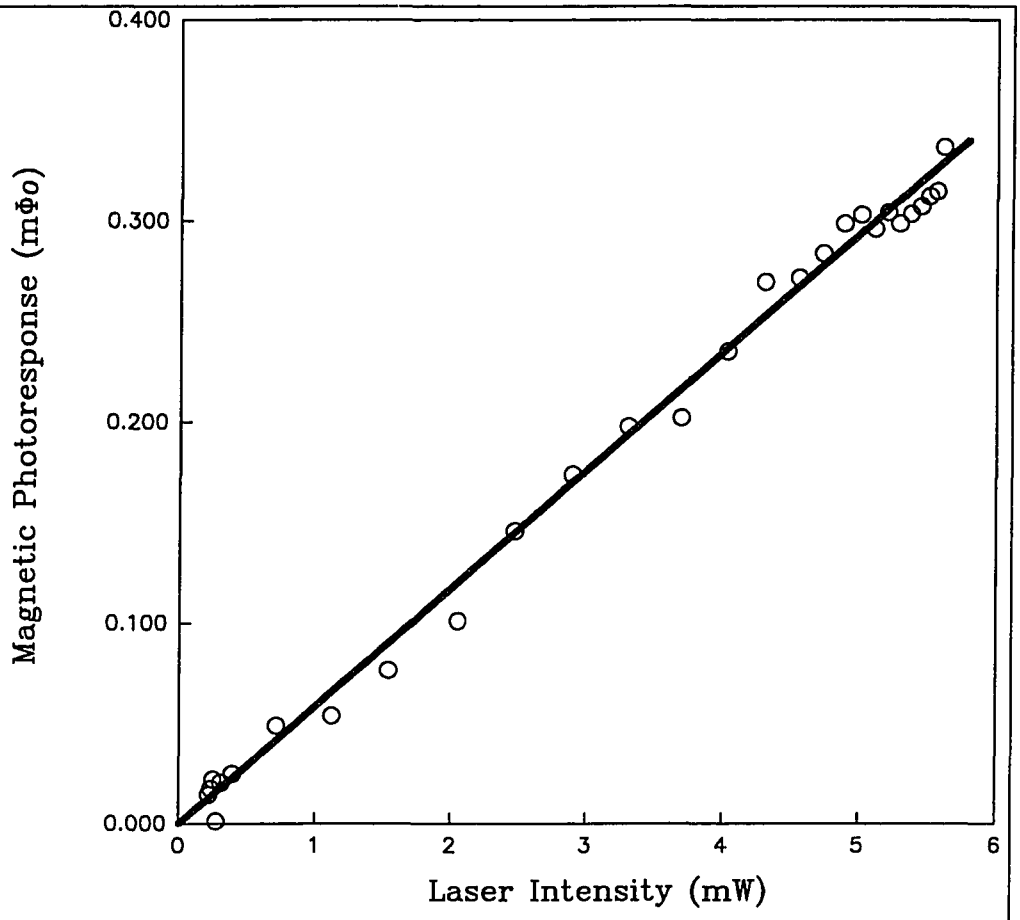

Fig. 4-4-5 Magnetic Photoresponse Data vs Light intensity on Nb-Al Array while the Temperature is held constant near 3.45 Kelvin

5: Summary

The array data has shown a magnetic photoresponse which is not readily explained by bulk heating models and has the temperature and intensity dependent properties of the photon-induced vortex-antivortex depairing effect. Whether the depairing effect is due to the intrinsic, intentionally induced properties of the array or whether all of the depairing is occurring at the site of some flaw in the array that was unintentionally created is unknown. In addition it should be noted that the amount of flux measured in the photoresponse

corresponds to one vortex - antivortex pair being depaired for only a tiny fraction of the incident photons, leaving a large gap to be filled before this mechanism could be used as a useful detector. Still, the data provides an indication that there is some very interesting physics going on below the Kosterlitz-Thouless transition temperature.

Above the Kosterlitz-Thouless transition temperature no flux signal that could be interpreted an a magnetic signal of the Kosterlitz-Thouless transition was seen. While the array has a Kosterlitz-Thouless transition, for reasons discussed earlier it is not observable by the SQUID.

As will be seen in the next chapter, the data is just the reverse for the In-InO_X sample which shows a strong magnetic signal from the Kosterlitz-Thouless vortices but an indecisive magnetic photoresponse. While both the arrays and the In-InO_X may be thought of as films consisting of superconducting islands coupled through non-superconducting material, there are several important differences. First of all the In-InO_X films have a much smaller granular structure with much tighter coupling between the grains. This allows for a higher density of vortex-antivortex pairs before recombination drives the mean free path so small that the vortices are not detectable. This may lead to the larger signal from the Kosterlitz-Thouless vortices.

The possible reasons why the In-InO_X photoresponse signal is not as readily seen will be covered in the next chapter.

V. EXPERIMENTAL RESULTS ON IN-INO_X

1: Experimental Setup

The experimental setup for the In-InO_X experiments was largely the same as for the array experiments, except for the samples. The flux transformer used was of the same type as used for the arrays, but some modifications were made to accommodate the change in sample size to 1 cm by 5 mm. The gradiometer was 3.5 mm wide by 5 mm long and centered over the array within ±1/2 mm. The gradiometer was thermally isolated from the array and was 100 - 500 μm above the array. This setup has previously been described in setion 5-1. The experimental setup is shown in figure 5-1-1.

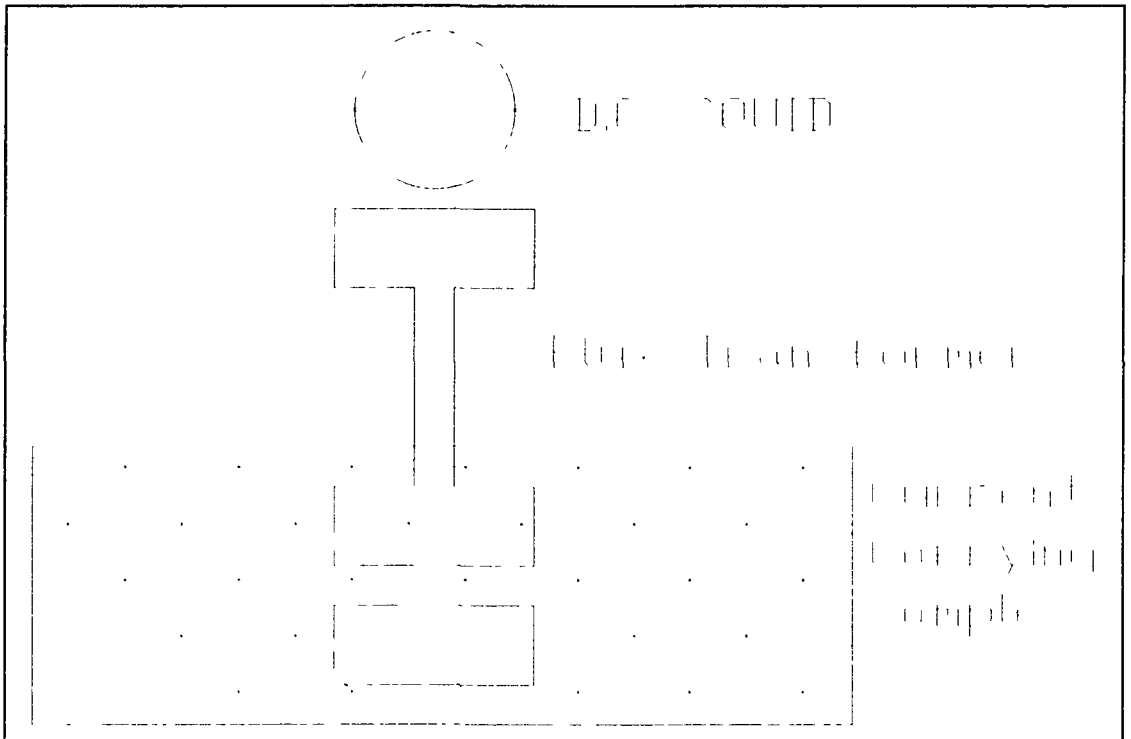

Fig. 5-1-1 Experimental Setup

2: Film Growth and Properties

The In-InO_X films were grown using an ion mill to sputter indium from a pure indium foil onto a glass substrate in an oxygen environment to thicknesses of 300-500 Å[54]. The superconducting transition occurs from about 3.6 K to 3.4 K, with a small resistive tail below 3.4 K. The sample also exhibits Kosterlitz-Thouless behavior near the superconducting transition[55]. Figure 5-2-1 shows the resistive transition of the sample.

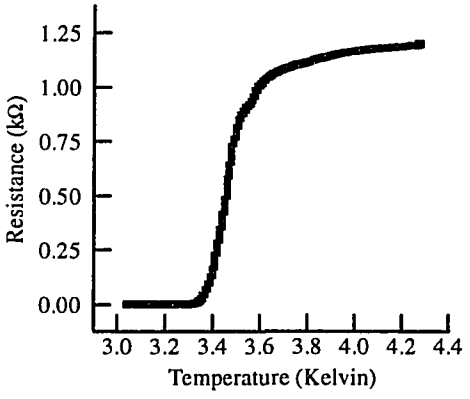

Fig. 5-2-1 Resistive Transition of the In-InO_X

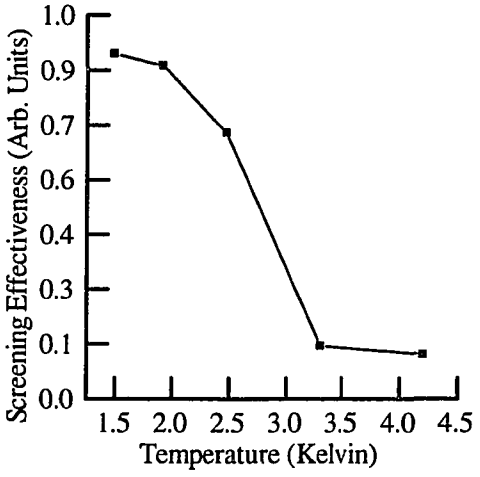

Fig. 5-2-2 Screening Effectiveness of In-InO_X vs. Temperature

Figure 5-2-2 shows the ability of the film to screen a magnetic field that is applied perpendicular to the sample at various temperatures. The screening capibility graph indicates the fraction of the magnetic flux that is screened by the film as a function of temperature. The screening effectiveness was measured using a magnetometer where a

54 A.F. Hebard and S. Nakahara, Appl. Phys. Lett. **41**, 1132 (1982)
55 A. T. Fiory, A.F. Hebard, and W.I. Glaberson, Phys. Rev. B **28**, 5075 (1983)

current carrying wire was placed along the center of the gradiometer, the same as for the arrays. The magnetic field from this wire induced a flux in the gradiometer and was then detected by the SQUID, as shown in figure 4-4-4 (in the array chapter). The magnetic flux measured by the SQUID was reduced at temperatures below Tc as the array began to magnetically shield the gradiometer from the applied flux. This figure shows an onset of the magnetic screening capability of the film around the same temperature as the base of the resistive transition, as would be expected.

3: Kosterlitz - Thouless Data

In the absence of light the signal has two major components: a component generated by the applied current, and a thermally activated vortex-antivortex pairs component. The component of the signal in the SQUID due to the transport current itself should be constant above the Kosterlitz-Thouless transition temperature (T_{KT}) and then drop off below as the film begins to screen magnetically. Using the temperature dependence for Kosterlitz-Thouless (K-T) vortex-antivortex pairs, the vortices should create a field gradient across the film at temperatures between the bulk transition temperature T_{CO} and T_{KT}, superimposing a dip in the field gradient vs. temperature curve due to current alone (see chapter 2, section 3 for the details of the calculation of the vortex contribution). A comparison of the actual signal (figure 5-3-2) and the expected signal (figure 5-3-1) shows a good qualitative agreement. The expected signal is calculated using three predetermined variables and one free variable. The predetermined variables are T_C, T_{KT} and the constraint that the "expected" result must agree with the magnetic screening curve below T_{KT}, while the free variable is a constant determining the magnitude of the vortex-antivortex contribution. The unexpected, sudden and temporary drop in the SQUID response to the applied current at 3.42 K corresponds to the drop in the dc SQUID value at

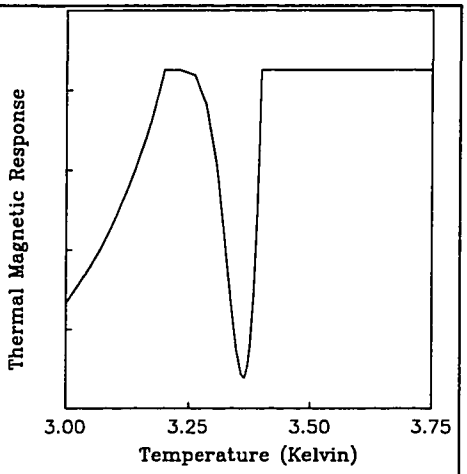

Fig. 5-3-1 Calculated Flux Through Gradiometer Due to Vortices vs Temperature

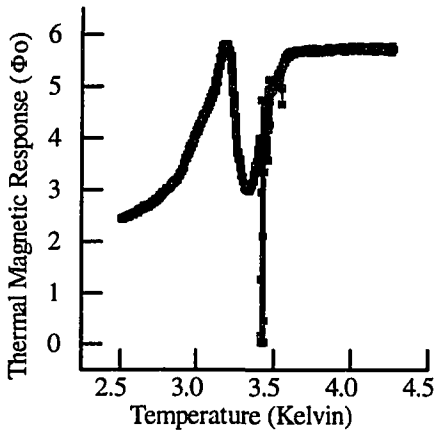

Fig. 5-3-2 Measured Magnetic Response to an Applied Current

the same temperature(see figure 5-3-3), and is due to a very high noise signal as the current realigns itself due to the rapidly changing resistance of the sample. This short aberration from the prediction may then be ignored.

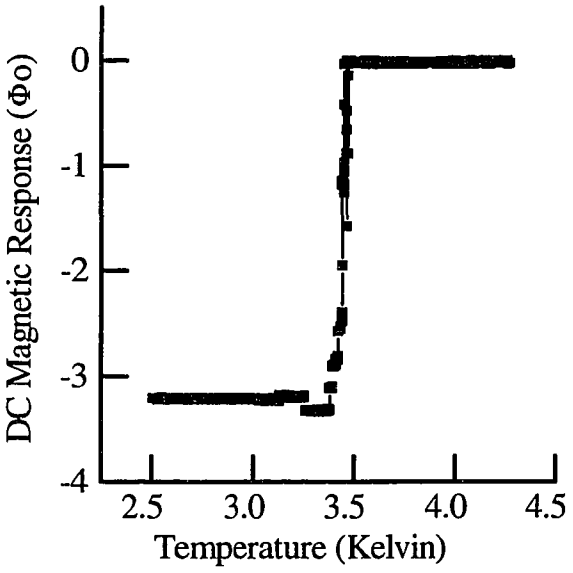

Fig. 5-3-3 Total SQUID Response to the ac and dc Current and Light

4: Photon - Induced Vortex - Antivortex Pair Data

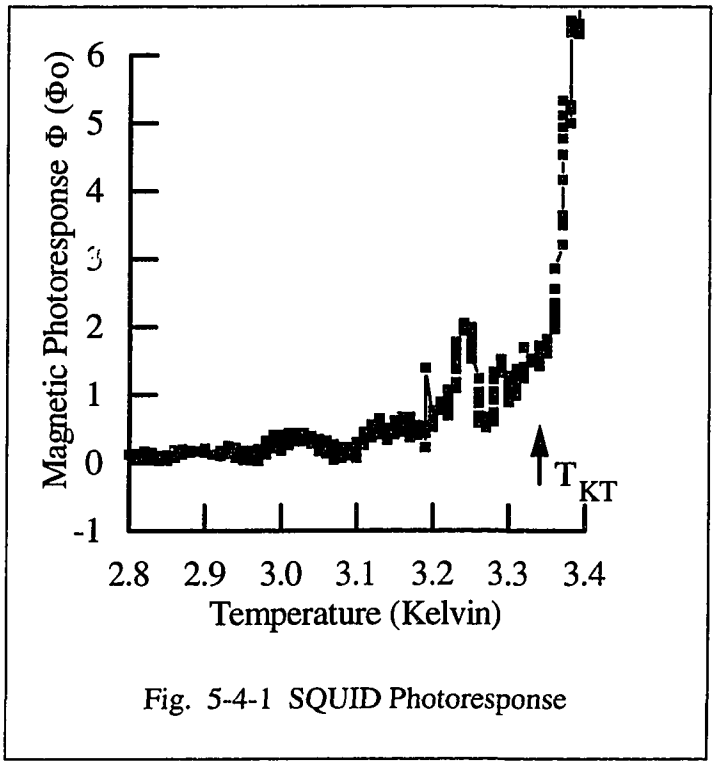

Fig. 5-4-1 SQUID Photoresponse

The magnetic response to applied light, as measured by the SQUID, is shown in figure 5-4-1. The very large signal corresponds to the high noise region associated with the superconducting transition and is above the temperature where photoinduced vortices should be observable by the experimental setup. Photoinduced vortices would be expected to be first observed at the base of the superconducting transition, dropping off rapidly as the temperature was changed in either direction. A signal has indeed been observed in this temperature region which is not readily explained by mere bulk heating effects. This signal begins at 3.3 K and remains above the noise threshold until about 3.0 K. While this signal is very encouraging as to the possibility of photoinduced vortices in In-InO_x, the features are not reproducible enough to allow for modeling and are unconvincing evidence for photoinduced vortex-antivortex pair breaking. A lack of a photoinduced voltage above what could be expected from heating alone does not rule out a low number of photoinduced vortex-antivortex pairs being depaired, but it casts further doubt onto the existence of photoinduced vortex-antivortex pairs being present in this sample.

5: Summary

In-InO_X has proven to be a very good material for observing thermally produced vortex-antivortex pairs. With a relatively short (compared to arrays) magnetic penetration length and a very large number of potential vortex sites, strong magnetic signals due to thermally induced vortex-antivortex pairs have been produced. Unfortunately, In-InO_X has proven to be a poor material for observing photoinduced vortex-antivortex pairs. These experiments should not, however, be taken as evidence against the photoinduced vortex-antivortex depairing theory as applied to granular In-InO_X due to the presence of a signal that may well be caused by photoinduced vortex-antivortex pairs. The magnetic field is clearly influenced by light irradiation in a way that is not easily explained by bulk heating. However, the signal vs. temperature curve is complicated and not reproducible run to run, preventing a convincing analysis. This could be due to a variety of reasons, including a low number of vortex-antivortex pairs actually depaired by photons causing statistical fluctuations, a current dependence strong enough to make run-to run variations in applied current give a slightly different production rate verses temperature, or any of several other possible causes. The presence of a strong signal from the thermally depaired Kosterlitz-Thouless vortices may also be masking a photoinduced signal. Then again it may not, and there may simply be no photoresponse other than that caused by simple heating.

In order to gain more sensitivity to signals below the Kosterlitz-Thouless transition, a different geometry was used on the $YBa_2Cu_3O_{7-X}$ samples. This new geometry will be discussed in the next chapter.

VI. EXPERIMENTAL RESULTS ON $YBa_2Cu_3O_{7-x}$

1: Experimental Setup

The experiments on $YBa_2Cu_3O_{7-x}$ were carried out with the sample magnetically coupled to a dc SQUID with a flux transformer, as shown in figure 6-1-1. The flux transformer and the dc SQUID were held at near 4.2 K while the $YBa_2Cu_3O_{7-x}$ sample was varied in temperature from 130 K to 6 K. The samples were patterned in the shape of an elongated loop. This elongated loop may be considered the union of two smaller loops, L1 and L2, connected in series. The actual sample shape was altered from the idealized shape in fig 6-1-1 in order to maximize the signal-noise ratio, but remained qualitatively equivalent to that shown in fig 6-1-1. The actual sample shape is shown in figures 6-1-2 and 6-1-3. A current, called the sample current, was injected between L1 and L2. A fiber

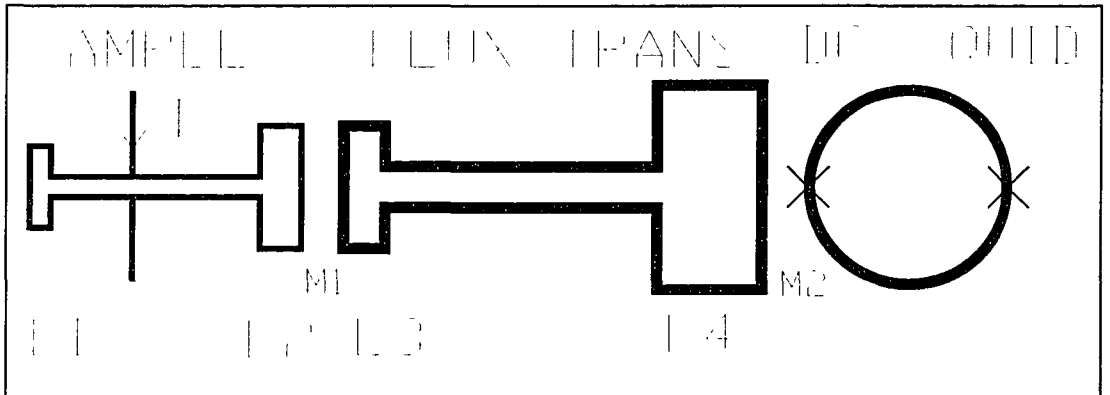

Fig. 6-1-1: Experimental Setup

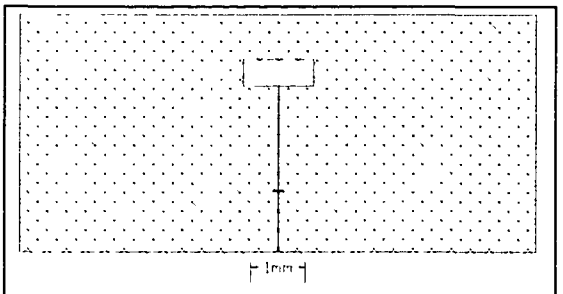

Fig. 6-1-2: Actual Sample Shape

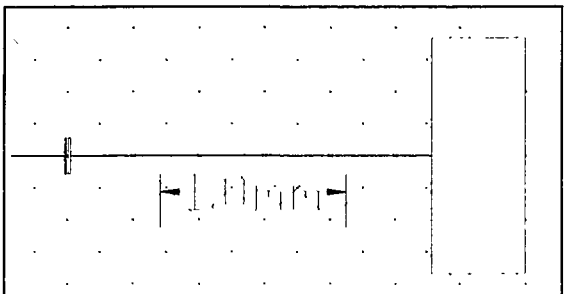

Fig. 6-1-3: Blowup of Actual Sample Shape (Rotated)

optic cable with a 100 μm diameter, shown in figure 6-1-4, that terminated 100 - 300 μm from the $YBa_2Cu_3O_{7-x}$ sample provided illumination for the photon-induced vortex-antivortex pair experiments. The illuminated spot covered the smaller loop of the sample, L1, but did not reach the larger loop of the sample, L2.

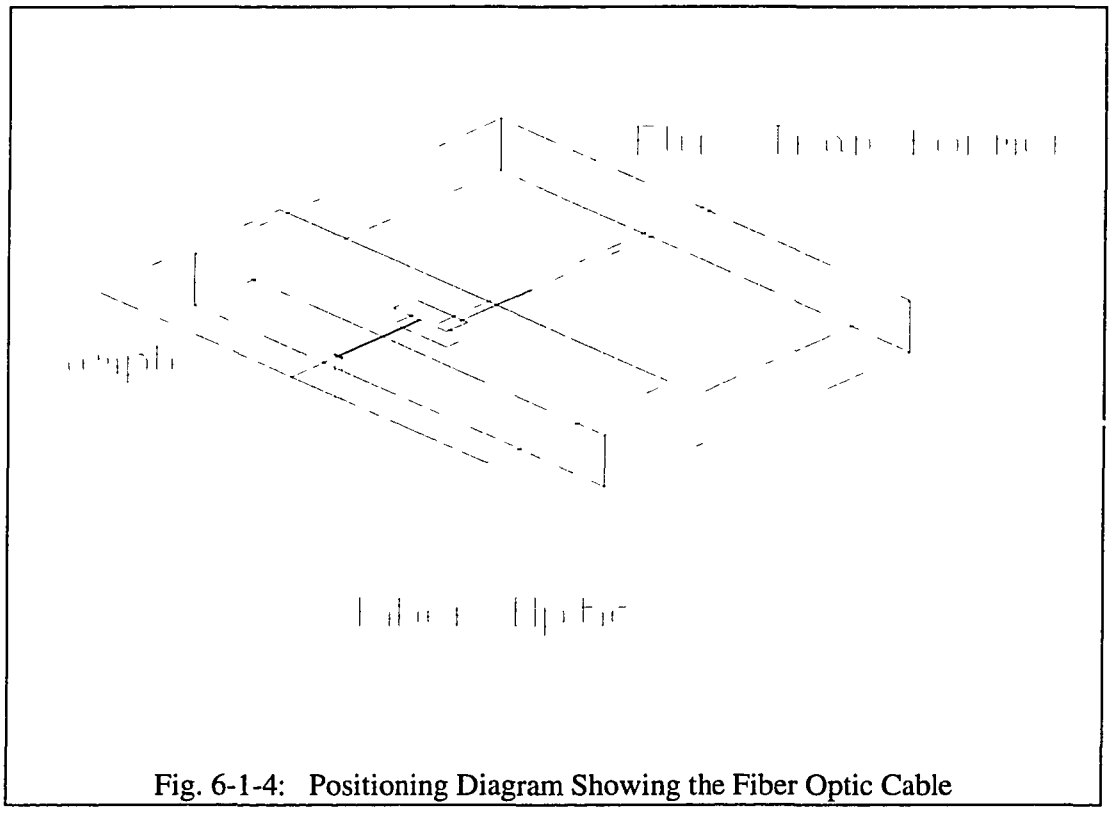

Fig. 6-1-4: Positioning Diagram Showing the Fiber Optic Cable

There are three temperature ranges of interest. The first range, consisting of all temperatures above T_c, is of little interest to this research and will be all but ignored. In this range, the current through the loop will divide according to the relative resistances of the two sides of the loop. Since the relative resistances of the two sides may be estimated from the geometry, this temperature regime is used to calibrate the efficiency of the flux transformers. This estimate is hampered by the fact that the coupling between the two loops will be different when they are both superconducting, but it provides a good baseline estimate.

The second range, from T_c to T_{KT}, is a bit more interesting due to the possibility of observing a magnetic signature from a Kosterlitz-Thouless transition. Unfortunately, in designing a geometry that is very sensitive below T_c, I designed a geometry that is very problematic in this temperature range. The source of the troubles using the "loop" geometry in this temperature range is that there are a large number of vortices that are in motion at the same time on both sides of the loop. While the flux through the loop is still dictated by the vortex motion, the large number of vortices in motion on both sides appears, when time averaged, as a resistance, and the time averaged flux through the loop is governed by the relative resistances of both loops again. Due to this no information is gained that could not have been more easily gained with a voltage measurement.

The third range, below T_{CO}, is the true range of interest. It is in this range that a vortex-antivortex depairing event may be seen clearly. In this range a single vortex-antivortex depairing event will result in a long lasting change in the flux through the loop and be easily detected[56]. It was for this range that the experimental geometry was designed. In this glorious range, the total flux through the loop is governed not by some resistance or effective resistance but by the quantum phase coherence around the loop. Here a single vortex-antivortex pair that separates and is moved off the edges of

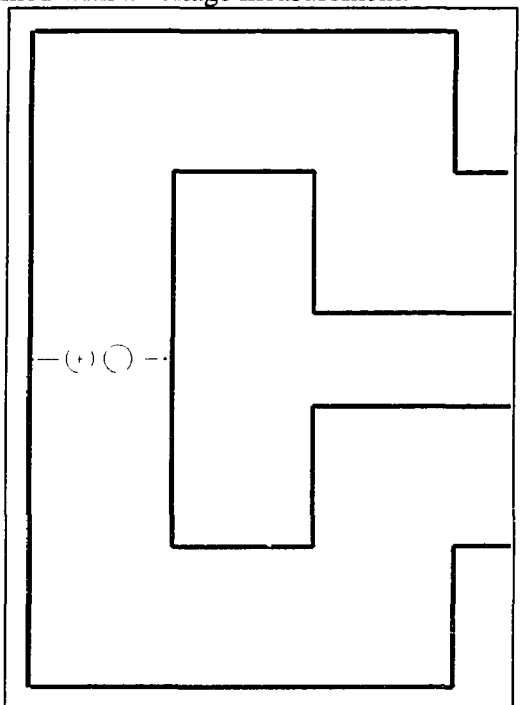

Fig. 6-1-5: Vortex Motion Diagram

56 R. Weinstein, In-Gann Chen, J. Liu, D. Parks, V. Selvanamickam and K. Salama, Appl. Phys. Lett. **56**, 1475 (1990)

the line will result in the permanent change of a full flux quantum through the loop. Should the vortex and antivortex only be moved halfway across the line the flux through the loop will still by changed by half of a flux quantum. It is this strength, that the changes are large and permanent, that allows very large sensitivities. In addition to very large sensitivities, it provides for a very reliable detection mechanism that does not rely on curve fitting or other error-prone data analysis methods - the vortices are there or they are not, and if they are there a change in flux through the loop will occur, if not no change in flux can occur in the loop.

The respective normal state resistances of L1 and L2 was estimated by the geometry of the loop and the change in flux through the SQUID and the sample current is varied was calculated by using the ratio of the resistances of L1 and L2. Since the ratio of the resistances of L1 and L2 should vary slowly above the onset of the superconducting transition, the ratio of the flux through the SQUID over the sample current should also change slowly above the onset of the superconducting transition, and this was in fact observed.

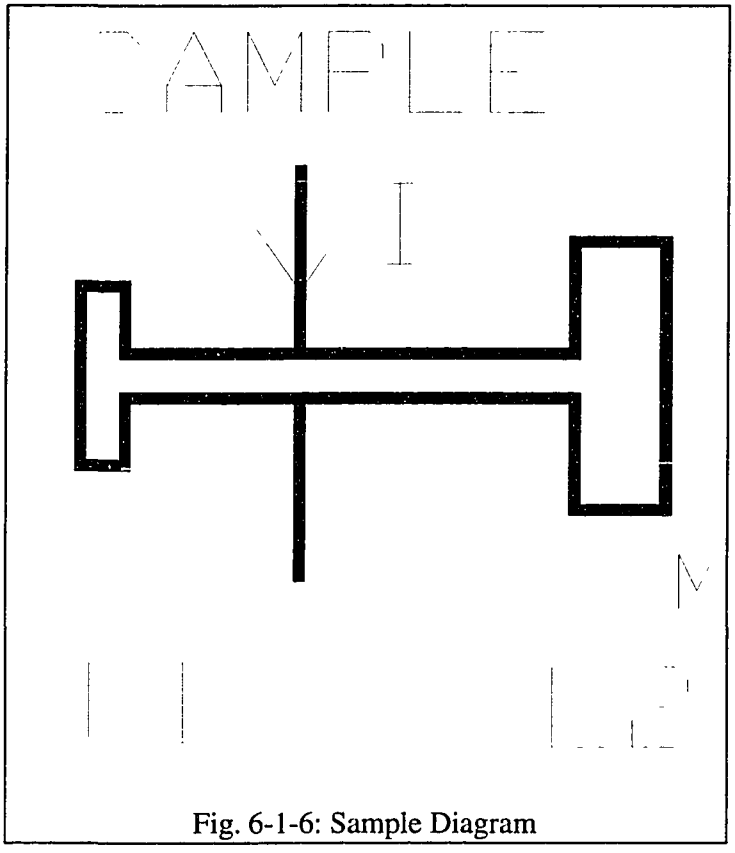

Fig. 6-1-6: Sample Diagram

The resistive transition of $YBa_2Cu_3O_{7-x}$ sample number two showed Kosterlitz-Thouless type behavior. For temperatures between T_{KT} and T_c the resistance of this

sample would then be dominated by the depairing of thermally activated vortex-antivortex pairs. Although a superconducting condensate is present throughout the sample loop, the supercurrent will not be able to hold the total flux through the loop at a constant value because the motion of the vortices will break the phase coherence around the loop. Due to the large number of vortices and antivortices in motion at any one time the effect of individual vortices is washed out by the time averaging of the signal. The time averaged sample current will then divide between L1 and L2 in such a way as to give the same voltage across L1 and L2, and the SQUID response to the sample current will be again governed by the effective resistances of L1 and L2. Since these effective resistances are current-dependent in this temperature region, the vortex-based nature of this resistance could be observable. This will be discussed in greater depth later.

Below T_{KT} the voltage across L1 and L2 drops to zero. The applied sample current will then divide so as to conserve the total flux through the sample loop. However, if a vortex-antivortex pair were to be depaired below T_c and the vortex and antivortex were driven off opposite edges of the film, a voltage spike would be induced across the superconductor. The voltage spike would have an amplitude V_1 given by $V_1 = \frac{\partial \Phi}{\partial t}$. Integrating over time gives a voltage spike of $2.07 \cdot 10^{-15}$ Volt-seconds. The supercurrent would the accelerate in such a way as to drive more current through the other side of the loop, keeping the voltage across both sides of the loop equal. The voltage across the other side of the loop is given by $V_2 = L\frac{\partial \vec{j}}{\partial t}$. Equating V1 and V2 and integrating over time will give a net change in the supercurrent so as to change the net flux through the loop by a single flux quantum. The direction of the change of flux is determined by whether the vortex-antivortex pair was depaired in L_1 or L_2. The net flux through the loop would then remain constant until an additional vortex event occurred or the temperature was increased

above T_c, again destroying the phase coherence around the loop. This argument hinges on the vortex-antivortex pair being driven apart once depaired, which implies that a minimum amount of current is maintained through the side of the loop where they are depaired. The minimum amount of current which is needed to depair a vortex-antivortex pair will depend on the initial separation of the vortices as well as several other factors. As the vortex-antivortex pairs are driven further apart, the current past them decreases to a maximum current drop of $\frac{\Phi_o}{L1 + L2}$, which occurs as the vortices reach the sides of the sample. So long as the current through the side of the loop in which the vortex-antivortex pair is created is larger than this when the vortex-antivortex pair is originally depaired, the current will continue to drive them apart. Since this effect is cumulative, if the vortex-antivortex pairs are all depaired on the same side of the loop, eventually the current through that side of the loop will drop below the depairing threshold and the depairing will cease.

This change in the flux through the sample loop would then be detected as a change in the flux through the SQUID, allowing for detection of a single vortex-antivortex event. Since the effect is cumulative for vortex-antivortex pairs all depaired on the same side of the loop it provides a very sensitive detection mechanism for detecting photo-induced vortex-antivortex pairs below T_c. At a given temperature below T_c, a current is applied through the sample and one side of the sample loop is illuminated. Any depaired vortex-antivortex pair that are separated by the current will then change the flux through the SQUID, and this change will be cumulative.

2: Film Growth and Properties

Three $YBa_2Cu_3O_{7-x}$ samples from two different films were used in this experiment. All the samples were 1000-1200 Å thick. The first film was grown by Laura

Greene's group using off-axis sputtering and I grew the second film by laser ablation. Sample 1 was a 1100 Å sputtered film which had a transition temperature in the upper eighties when measured by a transport technique and the lower eighties when measured using the Meissner effect. Sample two was the ablated film which has a transition temperature in the sixties. For sample three, the sputtered film was baked at 400°C. This resulted in a film whose superconducting transition was depressed to less than 20 K and had not achieved zero resistivity at 10 K.

The films were chosen with having a variety of oxygen contents as the primary goal[57]. The coupling between the adjacent layers in the $YBa_2Cu_3O_{7-x}$ crystal structure is reduced as the oxygen content is reduced[58,59,60]. At a sufficient reduction of oxygen, the adjacent layers become sufficiently decoupled for the $YBa_2Cu_3O_{7-x}$ behave as a collection of independent, stacked 2-d films[61,62,63]. When this is achieved, the energy required to form vortex-antivortex pairs drops dramatically because they may be contained in only a few atomic layers[64,65]. This reduction in the formation energy required gives a greatly enhanced likelihood of thermally generated bound vortex-antivortex pairs to be available for depairing. The energy of the absorbed photons will remain in the layer that absorbed the photon for a larger time as well, creating an electronic "hot spot" that is more likely to depair a vortex-antivortex pair. For these reasons the oxygen deficient $YBa_2Cu_3O_{7-x}$ is

---

57 B. Janossy, D. Prost, S. Pekker, and L. Fruchter, Physica C 181, **51** (1991)
58 P. Umadeve Muralidharan, T.R.Ramamohan, Phys Stat. Sol (a) **130**, 153 (1992)
59 B. Janossy, H. Gu, R. Cabanel, L. Fruchter, Physica C **193**, 344 (1992)
60 Hans Weber, Henrik Jeldotft Jensen, Phys. Rev. B **44**, 454 (1991)
61 L.N. Bulaevskii, S.V. Meshkov, and D. Feinberg, Phys. Rev. B **43**, 3728 (1991)
62 S.N. Artemenko and Yu. I. Latyshev, Modern Physics Letters B, **6**, 367 (1992)
63 T. Wang, K.M. Beauchamp, D.D. Berkley, B.R. Johnson, J. X. Liu, J. Xhang, and A.M. Goldman, Phys. Rev. B **43**, 8623 (1991)
64 J.M. Triscone, O. Fischer, O. Brunner, L. Antognazza, A.D. Kent, and M.B. Karkut, Phys. Rev. Lett. **64**, 804 (1990)
65 Baruch Horovitz, Phys. Rev. Lett. **67**, 378 (1991)

the most likely candidate among the $YBa_2Cu_3O_{7-x}$ varieties. $YBa_2Cu_3O_{7-x}$ samples that have higher oxygen contents were also tested for comparison.

The transport and magnetic transition data for the three $YBa_2Cu_3O_{7-x}$ samples is shown below. The transport data was taken with small currents and indicates the creation of low-resistivity percolation paths through the samples. The magnetic transition data measures the screening capability of the film using a two-coil method, which is functionally equivalent to the method described for the arrays and In-InO_x samples. The screening capibility graph indicates the fraction of the magnetic flux that is screened by the film as a function of temperature. This data indicates the temperature dependence of the superconducting transition of the bulk of the film, instead of a percolation path. In this way, the magnetic data is a better measure of overall film quality.

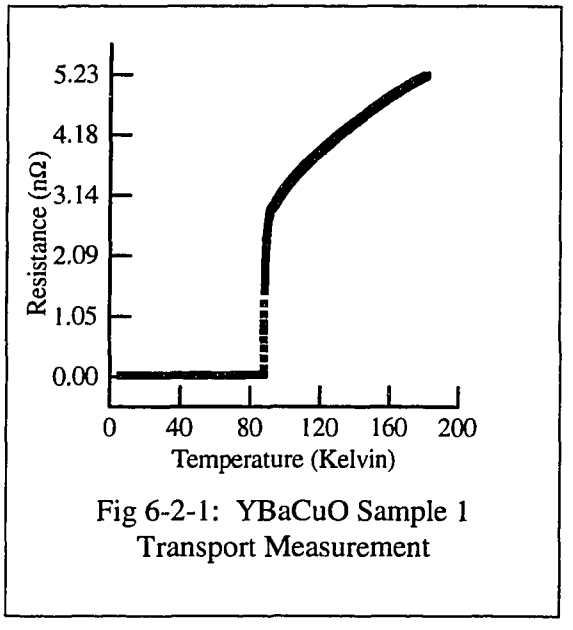

Fig 6-2-1: YBaCuO Sample 1
Transport Measurement

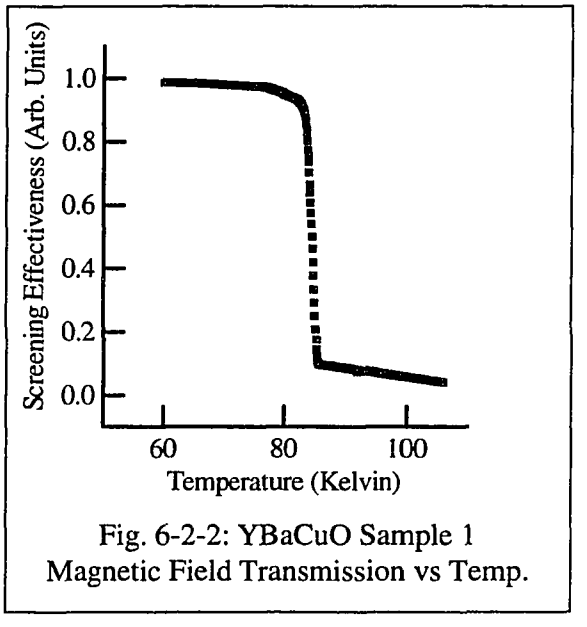

Fig. 6-2-2: YBaCuO Sample 1
Magnetic Field Transmission vs Temp.

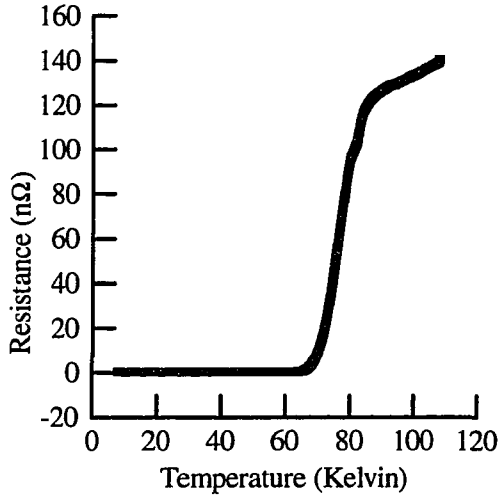

Fig. 6-2-3: YBaCuO Sample 2
Transport Measurement

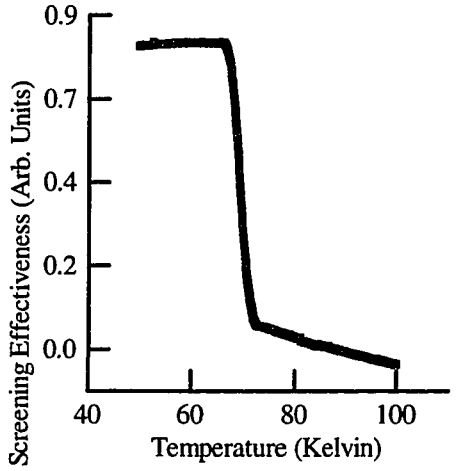

Fig. 6-2-4: YBaCuO Sample 2
Magnetic Field Transmission vs Temp.

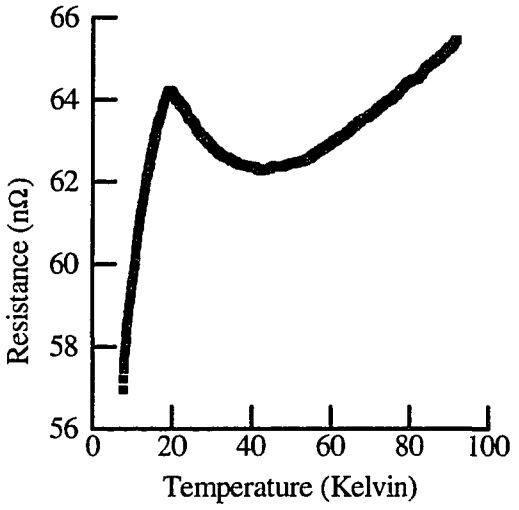

Fig. 6-2-5: YBaCuO Sample 3
Transport Measurement

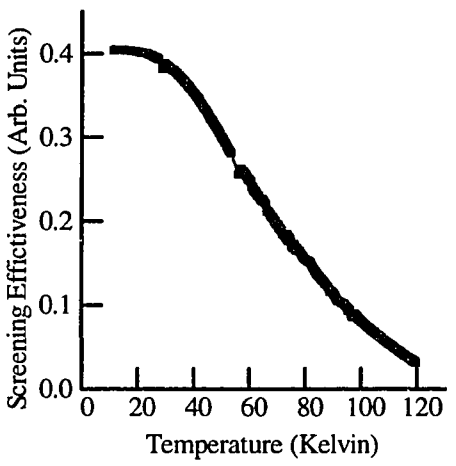

Fig. 6-2-6: YBaCuO Sample 3
Magnetic Field Transmission vs Temp.

Figures 6-2-1 and 6-2-2 correspond to the first sample. This sample was nearly fully oxygenated and I would expect fairly strong interplaner coupling. The base of the magnetic transition contains a small knee from about 75 K to around 82 K. This indicates a small percentage of the film consists of lower T_c $YBa_2Cu_3O_{7-x}$, however the very strong jump in the screening effectiveness at ~85 K indicates the film consists almost entirely of this phase of $YBa_2Cu_3O_{7-x}$.

Figures 6-2-3 and 6-2-4 correspond to the second sample. This sample is oxygen depleted (x ~ .3) and shows a T_c characteristic of a $YBa_2Cu_3O_{7-x}$ film with very poor interplaner coupling[66]. A careful look at the transport measurement (figure 6-2-3) shows a drop in resistance around 85 K, a leveling out for 1-2 K , then a smooth drop in resistance to zero resistivity. This indicates a small percentage of the film has perhaps a 85 K T_c, while the bulk of the film has the lower T_c. If you notc, the magnetic screening effectiveness shows no evidence of this, as it is very insensitive to the superconducting transition until nearly the entire film has transitioned. This gives an indication as to what a small fraction of the film in the first sample has a T_c below the main portion of the film.

Finally, figures 6-2-5 and 6-2-6 correspond to the third sample. This sample was strongly oxygen depleted and has the onset of a wide superconducting transition at ~20 K. Special note should be taken of the scale figure 6-2-6, which shows that the screening effectiveness of the film stays low at all temperatures. Below the onset of the superconducting transition the magnetic screening effectiveness does not increase, indicating a non uniform onset of superconductivity across the film.

---

66 J.R. Cooper, S.D. Obertelli, A. Carrington, J.W. Loram and W.Y. Liang, Physica C **185**, 1265 (1991)

3: Photon-Induced Vortex-Antivortex Pair Data

To search for photon-induced vortex-antivortex pairs experiments were run using a dc sample current and a chopped light source. The SQUID signal was measured at the chopping frequency of the light. Using this method the effect of the light on the flux through the ring is separated from the effect of the current, temperature drift and most of the noise. An estimate of the change in phonon temperature of the $YBa_2Cu_3O_{7-x}$ due to the incident light, ΔT, is made using the ac voltage signal of the sample and comparing it to the dc voltage change with temperature. This method requires an estimate of the relative resistances of the two loops that make up the ring, and a possible source of error enters here, but this error should be not more than a factor of three. This method of estimating the temperature increase to the incident light pulse gives a temperature increase of less than 3 mK. At temperatures below $T_{KT} + \Delta T$ the flux through the sample loop should be conserved. If any vortex-antivortex pairs were to be depaired and the vortex and antivortex moved in opposite directions across the film, a change in the total flux through the ring would occur. It should be emphasized that the

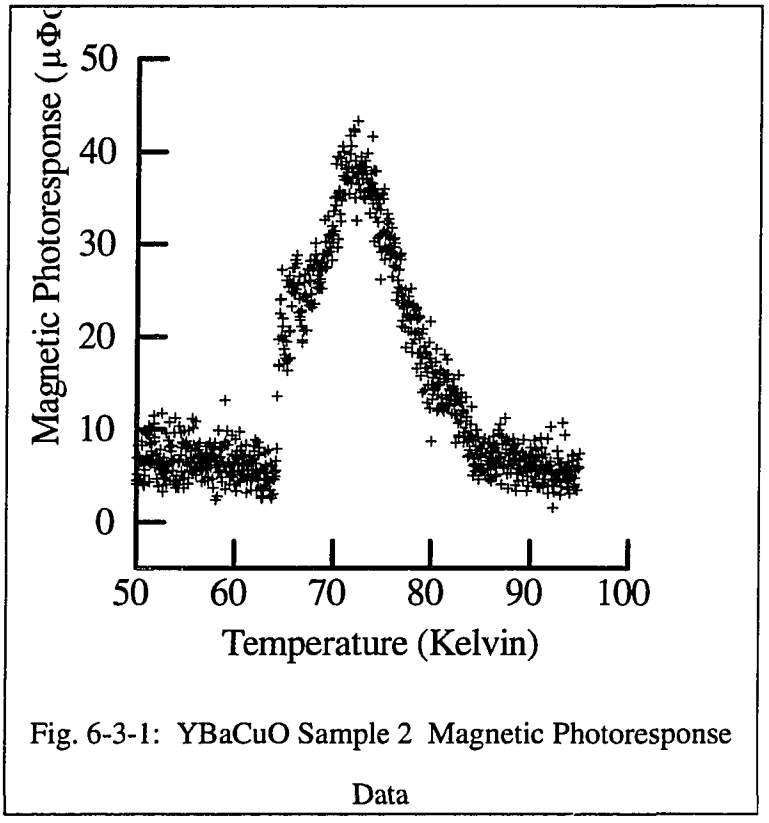

Fig. 6-3-1: YBaCuO Sample 2 Magnetic Photoresponse Data

vortex and antivortex need not be driven completely off the sides of the superconducting film to change the flux through the ring. The flux change in the ring will be approximately $\Phi_0 \cdot \frac{x}{w}$, where w is the width of the line and x is the change in the separation of the vortex and antivortex perpendicular to the line. In the temperature range of interest, below T_c, the small change in the phonon temperature of the superconducting film due to the light will have no effect on the flux through the loop and therefore any change in flux in this temperature range would be very strong evidence for photon-assisted depairing. Likewise, a lack of change in the flux through the ring in the presence of light irradiation would provide strong evidence that no vortex-antivortex pair breaking was occurring due to the light irradiation.

On the samples to date, no change in flux above the noise background has been observed in this temperature range. While the flux noise in the system precludes the conclusion that no vortex-antivortex pairs are being depaired by the light irradiation, an upper bound on the number of vortex-antivortex pairs that are depaired and driven to opposite sides of the film may be determined. The upper bound on the likelihood of any single photon depairing a vortex-antivortex pair and driving them to opposite sides of the film, L, is then given by $L = \frac{\text{Maximum signal}}{\text{Transformer efficiency} \cdot \text{\# of photons absorbed per cycle}}$. It should be emphasized that this is the likelihood of a single photon depairing a vortex-antivortex pair and driving them to opposite sides of the film, not a creation rate. The transformer efficiency was ~9% and the maximum signal at the SQUID was $4 \cdot 10^{-5}\ \Phi_0$. The number of photons striking the surface of the sample per cycle was set at about $1.3 \cdot 10^{12}$ photons. Not all of these photons will be absorbed in the $YBa_2Cu_3O_{7-x}$ film. Using very conservative values for the absorption rate, L is set at $3 \cdot 10^{-13}\ \frac{\text{pair}}{\text{photon}}$ at temperatures below T_c. This basically represents the efficiency of the entire system.

While this gives the likelihood that a single photon cause a vortex-antivortex pair to be completely separated, it is also possible that a vortex-antivortex pair is depaired by a photon and driven only part way across the line before being pinned. More rigorously put, the upper bound on the average distance that a photon causes a vortex-antivortex pair to be separated by is no larger than $3 \cdot 10^{-13}$ w, where w is the width of the film.

It is clearly unphysical to expect that the separation of a vortex-antivortex pair can be increased a distance less than the smallest characteristic length for the system at hand. For $YBa_2Cu_3O_{7-x}$ sample number two the smallest characteristic length of the system is the coherence length ~10 Å (pinning sites may occur on length scales on the order of the lattice spacing, which is also on the order of ~10Å). To calculate an absolute worst case upper bound, the distance of separation is taken at 10 Angstroms for all "depaired" vortex-antivortex pairs (although it is hard to talk about a vortex-antivortex pair only separated by an additional 1% of the magnetic penetration depth as being depaired). The width of the film is 20 microns, giving an upper bound on the fraction of photons that cause a vortex-antivortex pairs to be separated by even 10 Å to be $3 \times 10^{-13} \times \frac{20 \times 10^{-6}\,\mathrm{m}}{10^{-9}\,\mathrm{m}} = 6 \times 10^{-9}$. That would correspond to less than one vortex-antivortex pair being moved even 10 Angstroms for every 100 million photons.

At temperatures in the vicinity of or above T_{KT} the presence of thermally depaired vortex-antivortex pairs greatly complicates the interpretation of the data and makes the results far less reliable. Ideally the SQUID signal which is caused by the change in temperature of the sample due to the light could then be calculated and subtracted off the observed SQUID signal. The remaining ac SQUID signal could then be attributed to processes not dependent on the phonon temperature of the sample and would provide evidence for or against photon-assisted vortex-antivortex pair breaking. While the ac SQUID signal attributable to the chopped light merely raising the phonon temperature of

the sample may be estimated from the resistance verses temperature curve, the actual SQUID reading would also be a function of the critical current verses temperature curve, and is therefore difficult to determine. This, combined with the complicating presence of a large number of thermally induced vortices, makes the analysis used for the lower temperature case unreliable.

4: Kosterlitz-Thouless Data

While this experiment was not designed to look for Kosterlitz-Thouless generated vortices and is a poor geometry for doing so, it is interesting to look at the data in the temperature range of the Kosterlitz-Thouless transition and look for magnetic evidence of Kosterlitz-Thouless vortex-antivortex pairs.

The data taken while looking for a magnetic signal from a Kosterlitz-Thouless transition was taken using an ac sample current and no illumination. While a magnetic signal might also be expected from a dc sample current, an ac sample current was used to reduce the effect of SQUID noise and drift.

The measured signal then represents the flux through the SQUID due to the applied current. The change in the signal as the temperature is varied is a result of the applied current through the sample redistributing itself due to the changing resistance of both sides, any persistent current loops setup in the sample loop, and to the changing magnetic penetration depth of the sample loop. As the magnetic penetration depth of the sample loop decreases, the currents in the portion of the sample that couples the flux transformer redistribute in such a way as to couple more flux into the SQUID per unit of current.

In the absence of magnetic vortices, two features are expected. The first major change in the signal strength is due to the changing resistance and the second is due to the changing coupling constant as the magnetic penetration depth changes. Before speculating

about the presence of thermally produced vortices from the data, an attempt should be made to explain the data from using only the resistance and inductance of the sample. A phenomenological model was made using only the resistances of the two sides of the loop, the inductances of the two sides of the loop, and the magnetic screening of the samples as measured using a two coil experiment. The inductances of the loops were fixed and the resistances were allowed to vary with temperature. It was assumed that for temperatures where there was any measurable resistance the current divided according to the relative resistances of the two loops of the sample, and below that temperature the current divided according to the relative inductances. A smooth transition between these two states was obtained by overlapping the two criteria with a weighting factor that changed smoothly but rapidly at the base of the superconducting transition. The coupling of the sample to the SQUID is affected by the temperature dependence of the magnetic penetration depth of the samples, so the magnetic screening data was used to account for this. This effect is responsible for the peak in the calculated curves for each of the samples. The model was constrained to match the magnetic screening vs temperature as well as the resistance vs temperature curves of the sample. For this reason, the model gives different results for sample 1 and sample 2 due to their different resistance vs temperature profiles and magnetic screening vs temperature profiles.

Figures 6-4-1 and 6-4-3 show the flux-signal data vs temperature and the theoretical fit of the data. Figures 6-4-2 and 6-4-4, which show the resistive and magnetic transitions, have been included for reference.

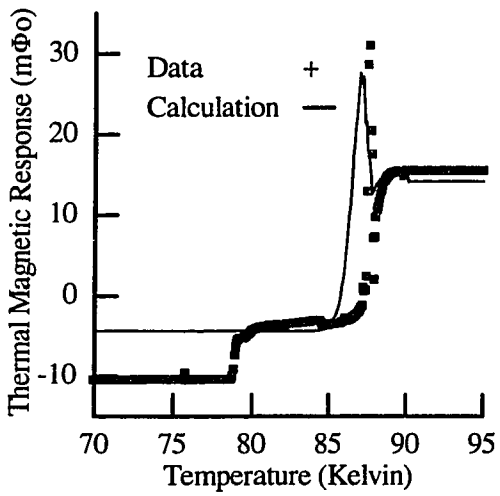

Fig. 6-4-1: YBaCuO Sample 1

Measured Magnetic Response to an Applied Current

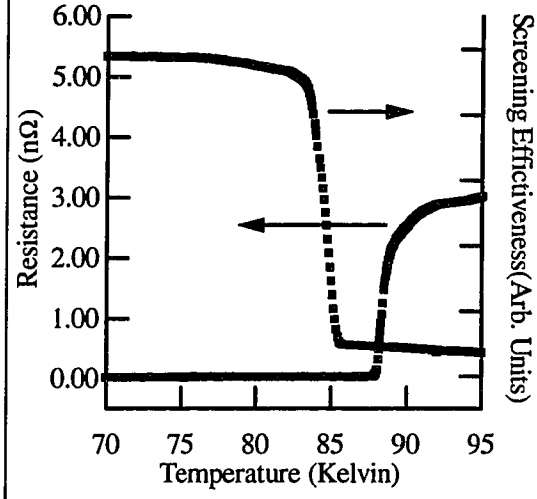

Fig. 6-4-2: YBaCuO Sample 1

Transport and Magnetic Transition

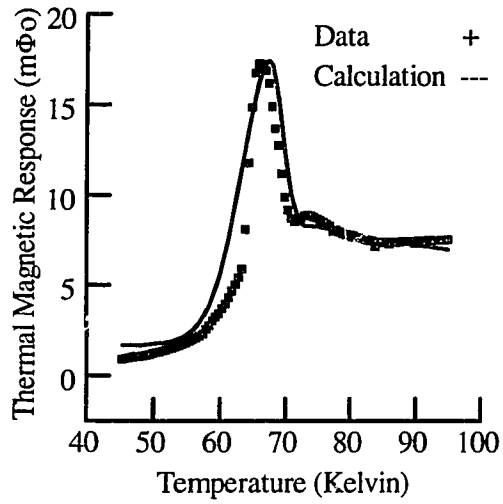

Fig. 6-4-3: YBaCuO Sample 2

Measured Magnetic Response to an Applied Current

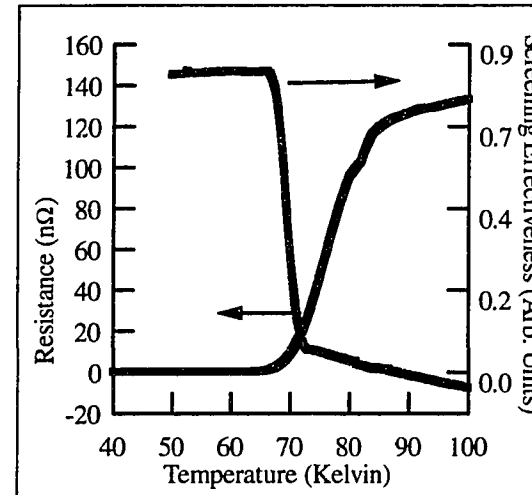

Fig. 6-4-4: YBaCuO Sample 2

Transport and Magnetic Transition

While superior fits to the data have been made by using vortex-antivortex depairing terms, there is enough uncertainty in the parameters to allow a full explanation of the sample 2 data without them. It should be remembered that the two sides of the sample loop may have slightly different resistivity vs temperature functions which would certainly affect this data, so a perfect fit is not expected. While this fit by no means rules out the presence of thermally induced vortex-antivortex pairs, the ability to model all qualitative features of the data fairly closely rules out using this data as an indication of thermally created vortex-antivortex pairs.

The resistance and magnetic screening transitions for sample 1 are separated by several degrees. This is most easily explained by an inhomogeneous film: the resistance will drop to zero when a percolation path is established, but the screening does not begin until nearly the entire film is superconducting.

For sample 1, the jump in flux at 79 K is not explained by the resistance vs temperature data, but there is a small feature in the magnetic screening data that corresponds to this jump. While the model does not fit this feature, the model assumes a fixed ratio of the inductances of the loops. This assumption is clearly incorrect given this jump so far below the resistive transition.

The sharp peak at 87 K corresponds to the onset of the magnetic (screening) transition of the film. While the model does not quantitatively explain the sharpness of the peak, the increased magnetic coupling of the sample to the SQUID due to the onset of magnetic screening accounts qualitatively for this peak. In addition, the resistance vs temperature curve is very sharp in this region and a small difference in the T_c of the two sides of the loop could cause such a sharp, large peak easily.

Now the explanations for these two unaccounted for features may not be satisfying, but they do not need to be - the existence of any plausible explanation for these features that does not resort to vortices precludes the possibility of citing them as evidence for

thermally created vortex-antivortex pairs, particularly in the absence of a compelling vortex model that models these features with a low number of free parameters. Furthermore, sample 1 is the nearly fully oxygenated sample where thermally created vortex-antivortex pairs are far less likely than in sample 2, which is modeled more convincingly without resort to vortices.

The data for sample 3, shown in fig. 6-4-5, shows no interesting features above 30 degrees, as would be expected for a sample with no superconducting transition.

This leaves the question of whether the data shows magnetic evidence of Kosterlitz-Thouless vortices in $YBa_2Cu_3O_{7-x}$ unanswered, which is unfortunate but should not be unexpected since the experiment was not designed to detect vortex-antivortex pairs depairings above T_c.

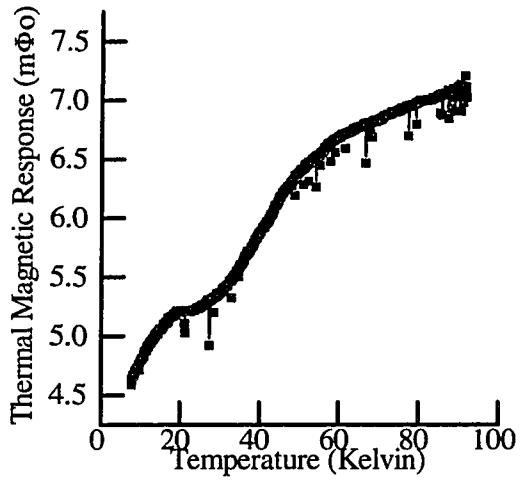

Fig. 6-4-5: YBaCuO Sample 3 Measured Magnetic Response to an Applied Current

5: Summary

While the sample geometry does not allow for much of an analysis of the data in the temperature region where thermally generated free vortices occur, it is a very powerful geometry for determining the presence or absence of light-induced vortex motion below the resistive transition. In addition to the analysis done earlier showing that below T_c the photon-induced vortex-antivortex pair breaking does not readily occur in high quality, reduced oxygen $YBa_2Cu_3O_{7-x}$ below T_c, it should be noted that the upper bounds derived

earlier apply to any photon-induced phenomena that would cause vortex motion, not only to the case of photon-induced vortex-antivortex pair breaking by the mechanism described in the theory chapter. The data then provides strong evidence against photon-induced vortex-antivortex pair breaking in the $YBa_2Cu_3O_{7-x}$ samples studied. This casts doubt on whether non-granular $YBa_2Cu_3O_{7-x}$ films could be made to work as detectors using the photon-induced vortex-antivortex mechanism, as well as whether the non-bolometric photoinduced voltages are caused by photoinduced vortices.

VII. CONCLUDING REMARKS

1: Photoinduced Vortex-Antivortex Depairing

The array data has provided evidence that vortex-antivortex depairing is indeed a plausible explanation for the nonbolometric photoresponse seen in a variety of granular films. This did not carry over into finding evidence for vortex-antivortex depairing in the In-InO_X and $YBa_2Cu_3O_{7-x}$ films. More detailed summaries for the separate samples are located at the end of the appropriate chapters.

One further test not previously mentioned but done on the $YBa_2Cu_3O_{7-x}$ was to monitor the flux through the loop vs time in the presence of light. It was found that the rate of change of the flux was not affected by the presence of the light. Since the effect of vortex motion is cumulative, this provides an even more stringent standard of the lack of vortex-antivortex depairing due to the presence of the light. This supports those arguing for a bolometric explanation for the fast photoresponse in $YBa_2Cu_3O_{7-x}$[67].

2: Kosterlitz-Thouless Transition

These experiments also provided an opportunity to look for a magnetic signal from the Kosterlitz-Thouless transition in the In-InO_X granular system, and that magnetic signature was indeed found. This, combined with the work of Hue Gong Lee, DA. Rudman, J.C. Garland and D.J. VanHarlingen[68,69] should put to rest the doubts about the

---

67 F.A. Hegmann, J.S. Preston, Phys. Rev. Lett. **48**, 16023 (1993)
68 Hu Jong Lee, D.A. Rudman, and J.C. Garland, Phys. Rev. Lett. **55**, 2051 (1985)
69 J.C. Garland, D.J. VanHarlingen, Phys. Rev. Lett. **55**, 2047 (1985)

Kosterlitz-Thouless theory of vortex unbinding raised by Bancel and Grey[70]. An evaluation of this data is in the In-InO_x chapter.

3: Detector Possibilities

The detector possibilities are promising because while bolometers have the ability to have high resolution they are slow (in the millisecond regime) where this method has the ability to achieve fast response times (microsecond regime) and high resolution[71]. In order to achieve high resolution with this method, superconducting films that are more efficient at converting photons into depaired vortex-antivortex pairs must be developed. In order to achieve this, a deeper understanding of the film properties that enable the photon-induced vortex-antivortex depairing to occur is needed.

One rather large impediment to the practical use of this phenomenon as a detector is the recent improvements in bolometer technology. Daniel E. Prober of Yale University has recently done some very interesting work in getting around the seemingly inherent slowness of traditional bolometers. This work appears as if it may lead to sensitive bolometers that may work faster than vortex-antivortex depairing could. This is a very exciting development and I would encourage anyone interested in developing vortex-antivortex depairing as a detector to explore the state of the art in this field as well.

---

70 P.A. Bancel and K. E. Grey, Phys. Rev. Lett. **46**, 148 (1981)

71 H. S. Kwok, L. Shi, J.P. Zheng, S.Y. Dong, Y. Pang, and P. N. Prasad, SPIE **1394**, 196 (1990)

4: Possible Future Directions

There are two major directions possible for future work in this field: detector development and understanding the mechanism. Personally, I do not believe that films that will have a reasonable detection efficiency can be developed without a further understanding of the structures that enable photon-induced vortex-antivortex depairing. The most useful next step would be the development of NbN-BN cermet film samples for testing for photon induced vortex-antivortex depairing. These films have shown a strong non-bolometric photoresponse that is flat far below T_c and would be a very useful next sample in order to correlate a voltage signal to the magnetic signal[72,73]. Unfortunately, these films are non-trivial to develop, however efforts are currently underway to produce them for the photon-induced vortex-antivortex pair experiments.

---

72 M. Leung, U. Strom, J.C. Culbertson, J.H. Claassen, S.A. Wolf, and R.W. Simon, Appl. Phys. Lett. **50**, 1691 (1987)

73 R.W. Simon, B.J. Dalrymple, D. Van Vechten, W.W. Fuller, and S.A. Wolf, Phys. Rev. B **36**, 1962 (1987)

APPENDIX A: MAGNETIC FIELD CALCULATION

This appendix contains a calculation addressing the vortex dynamics and related magnetic field over a superconducting line. The vortex dynamics calculation is needed for both the gradiometer and the ring experiments, where the resultant magnetic field directly over the line is relevant for understanding the data on the arrays and In-InO_x where the gradient of the magnetic field over the superconducting line is measured.

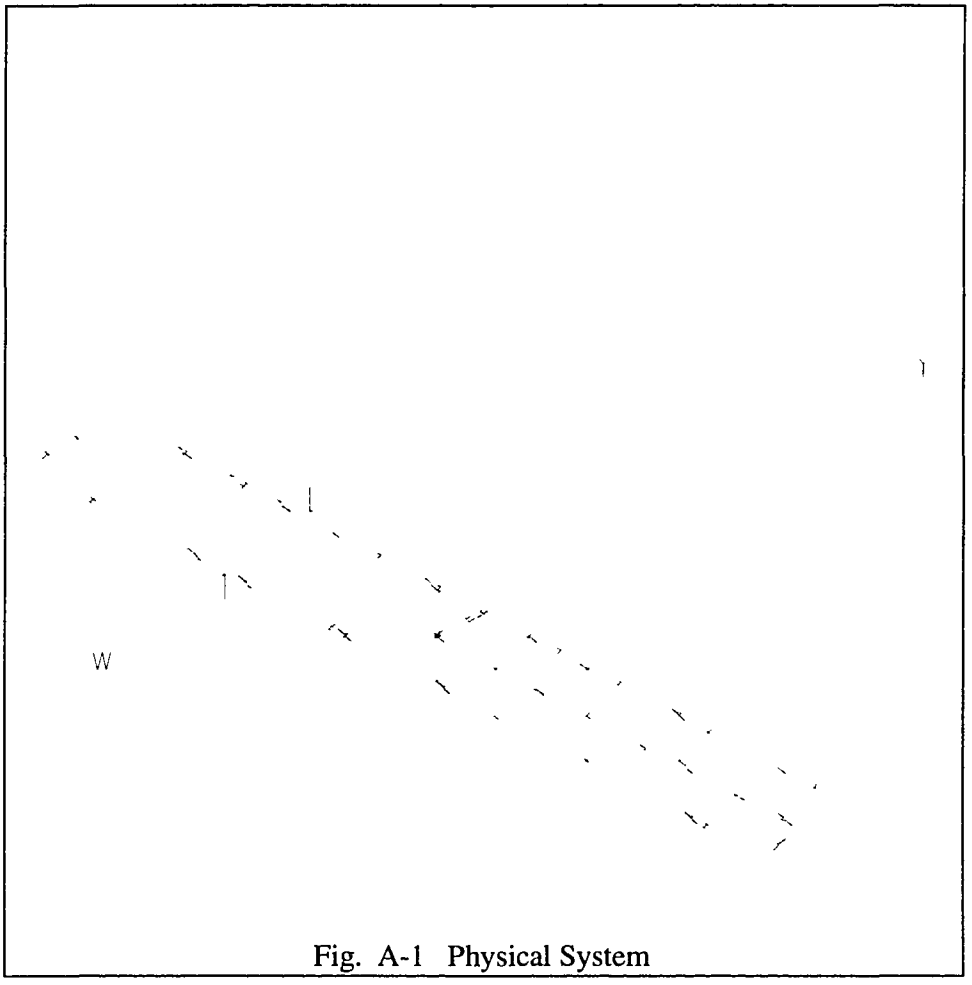

Fig. A-1 Physical System

The average field due to vortices is $H_v(\vec{r}) = \Phi_o[n^+(\vec{r}) - n^-(\vec{r})]$ and the equations of continuity describing the density of vortices and antivortices are

$$\frac{\partial n^+(\vec{r},t,T)}{\partial t} + \frac{\partial(n^+(\vec{r},t,T)v^+)}{\partial y} = G^+(\vec{r},T) - k(T)n^+(\vec{r},t,T)n^-(\vec{r},t,T)$$

$$\frac{\partial n^-(\vec{r},t,T)}{\partial t} + \frac{\partial(n^-(\vec{r},t,T)v^-)}{\partial y} = G^-(\vec{r},T) - k(T)n^+(\vec{r},t,T)n^-(\vec{r},t,T)$$

where n^+ and n^- are functions of position, time and temperature.

The variables used are as follows:

H_v = Net field due to vortices

H_j = Field due to current in the film

$n^{\pm}(\vec{r},t,T)$ = Areal density of vortices (antivortices)

$v^{\pm}$ = $\pm$ Vortex velocity in the y direction

$G^{\pm}(\vec{r},T)$ = $\pm$ Vortex - Antivortex depairing rate

$R(\vec{r},T)$ = vortex - antivortex recombination rate

$k(T) \equiv \frac{R(\vec{r},T)}{n^+(\vec{r},t,T)n^-(\vec{r},t,T)}$, where $k(T)$ is the recombination constant

This gives the most general vortex distribution. For the experiment at hand the most general solution possible is not required, and the following experimental conditions are imposed on the solution:

1: $\frac{\partial n^+(\vec{r},t,T)}{\partial t} = \frac{\partial n^-(\vec{r},t,T)}{\partial t} = 0$ Steady state condition

2:	$v^+ = -v^- = v,\ v \neq v(y)$	For a given current density vortices and antivortices have equal and opposite velocities, and the current density is constant across the line.
3:	$G^+ = G^-,\ G \neq G(r)$	Vortex and antivortex creation (depairing) rates are equal (they are made in pairs) and this creation rate is held constant across the line. While the creation rates in an actual experiment vary due to temperature differences across the line, uneven illumination or other nonuniformities, for the ease of calculation these are ignored.
4:	$n^+(\vec{r},t,T)(y=0) = n^-(\vec{r},t,T)(y=0)$	This is true by symmetry in the case of no external magnetic field.
5:	For $-w/2 \leq y \leq w/2$, $n^+(\vec{r},t,T)$ and $n^-(\vec{r},t,T)$ are finite.	An infinite vortex or antivortex density is unphysical.

In addition to the experimental conditions placed on the system, a single boundary condition is needed. This boundary condition is that $n^+(y = -w/2) = n^-(y = w/2) = \gamma$ and stipulates the density of vortices on the edge from which they are being driven. Their density at this edge, γ, will be affected by the rate at which vortices are being absorbed at the edge of the film; for no vortices being absorbed at the edge $\gamma = 0$, and for the same number of vortices entering as leaving γ will equal the number of vortices in the center of the film - this is the infinite film limit.

Applying experimental condition one: $\frac{\partial n^+(\vec{r},t,T)}{\partial t} = \frac{\partial n^-(\vec{r},t,T)}{\partial t} = 0$:

$$\frac{\partial(n^+(\vec{r},t,T)v^+)}{\partial y} = G^+(\vec{r},T) - k(T)n^+(\vec{r},t,T)n^-(\vec{r},t,T)$$

$$\frac{\partial(n^-(\vec{r},t,T)v^-)}{\partial y} = G^-(\vec{r},T) - k(T)n^+(\vec{r},t,T)n^-(\vec{r},t,T)$$

Applying experimental condition two: $v^+ = -v^- = v, \quad v \neq v(y)$:

$$\partial_y n^+(\vec{r},t,T) = \frac{G^+(\vec{r},T)}{v} - \frac{k(T)}{v}n^+(\vec{r},t,T)n^-(\vec{r},t,T)$$

$$\partial_y n^-(\vec{r},t,T) = -\frac{G^-(\vec{r},T)}{v} + \frac{k(T)}{v}n^+(\vec{r},t,T)n^-(\vec{r},t,T)$$

Applying experimental condition three: $G^{\pm} = G^{\mp}, \quad G \neq G(r)$:

$$\partial_y n^+(\vec{r},t,T) = \frac{G(T)}{v} - \frac{k(T)}{v}n^{+(\vec{r},t,T)}n^-(\vec{r},t,T)$$

$$\partial_y n^-(\vec{r},t,T) = -\frac{G(T)}{v} + \frac{k(T)}{v}n^+(\vec{r},t,T)n^-(\vec{r},t,T)$$

$$\partial_y n^+(\vec{r},t,T) = -\partial_y n^-(\vec{r},t,T)$$

Applying experimental condition four, $n^{\pm}(\vec{r},t,T)(y=0) = n^{\mp}(\vec{r},t,T)(y=0)$

Combining this condition with $\partial_y n^+(\vec{r},t,T) = -\partial_y n^-(\vec{r},t,T)$ gives the relation that $n^+ + n^- =$ constant.

Making the following substitutions [74]

$$n^+(\vec{r},t,T) + n^-(\vec{r},t,T) = N,\ n^+(\vec{r},t,T) - n^-(\vec{r},t,T) = D(y),\ z = \left[\frac{\sqrt{Gk}}{v}\right]y\ ,$$

$$W = \left[\frac{\sqrt{Gk}}{v}\right]\frac{w}{2}\ ,\ n = \frac{N}{\sqrt{4G/k}}\ ,\ \text{and}\ f(z) = \frac{D(y)}{N}\ \text{gives}$$

$$v\frac{\partial D(y)}{\partial y} = 2\left[G - \frac{k}{4}(N^2 - D^2(y))\right]$$

$$\sqrt{Gk}\,N\frac{\partial f(z)}{\partial z} = 2G\left[1 - \frac{k}{4G}N^2(1 - f^2(z))\right]$$

$$\sqrt{Gk}\,n\sqrt{\frac{4G}{k}}\frac{\partial f(z)}{\partial z} = 2G\left[1 - \frac{k}{4G}N^2(1 - f^2(z))\right]$$

$$n\frac{\partial f(z)}{\partial z} = \left[1 - n^2(1 - f^2(z))\right]$$

Noting that f(z) must be positive, this gives:

$$\text{for } n < 1, \qquad f(z) = \sqrt{\frac{1}{n^2} - 1}\,\tan\left[\sqrt{1 - n^2}\,(z - z_o)\right]$$

$$\text{for } n = 1, \qquad f(z) = (z_o - z)^{-1}$$

$$\text{for } n > 1, \qquad f(z) = -\sqrt{1 - \frac{1}{n^2}}\,\tanh\left[\sqrt{n^2 - 1}\,(z - z_o)\right]$$

By symmetry z_o must be 0. The n=1 solution may be rejected because it results in a singularity in the center of the strip. The n>1 solution is unphysical because it implies a net loss of vortices in the center of the superconducting film.

$$\text{for } n < 1, \qquad f(z) = \sqrt{\frac{1}{n^2} - 1}\,\tan\left[\sqrt{1 - n^2}\,(z)\right]$$

---

74 A. Leggett, private communication. This communication, in addition to suggesting these substitutions, greatly helped with the rest of this calculation

$$f(z) = \sqrt{\frac{1}{\frac{N^2}{4G/k}} - 1}\tan\left[\sqrt{1 - \frac{N^2}{4G/k}}(z)\right]$$

$$f(z) = \sqrt{\frac{4G}{kN^2} - 1}\tan\left[\sqrt{1 - \frac{kN^2}{4G}}(z)\right]$$

$$D\left(\frac{\sqrt{Gk}}{v}y\right) = N\sqrt{\frac{4G}{kN^2} - 1}\tan\left[\sqrt{1 - \frac{kN^2}{4G}}\frac{\sqrt{Gk}}{v}y\right]$$

Applying experimental condition five, For $-w/2 \le y \le w/2$, $n^{\pm}(\bar{r},t,T)$ and $n^{\mp}(\bar{r},t,T)$ are finite

The above equation satisfys this condition.

$$D\left(\frac{\sqrt{Gk}}{v}y\right) = N\sqrt{\frac{4G}{kN^2} - 1}\tan\left[\sqrt{1 - \frac{kN^2}{4G}}\frac{\sqrt{Gk}}{v}y\right]$$

Applying the boundary condition, $n^{\pm}(y = -w/2) = n^{\mp}(y = w/2) = \gamma$:

For $\gamma = 0$, $f(z) = -f(z) = 1$ when $y = \pm w/2$.

Solving for $\gamma = 0$, the vortex (m_i) and antivortex (n_i) densities as a function of position across the line are shown in figure A-2. The magnetic field strength as a function of position across the line is shown in figure A-3. Gradient in the density of vortices and antivortices is greatest at either edge of the line, as would be expected due to the drop in recombination events at either side. Near the middle the gradient in the vortex density drops as the vortex recombination rate approaches the vortex generation rate. Figures A-2 and A-3 were created with the following parameters: vortex velocity = 10^4 m/s, vortex generation rate g = 10^4 vortices/(second*m_2), vortex recombination constant k = 10^5 m^2/(vortex*second), and a line width of 100 microns.

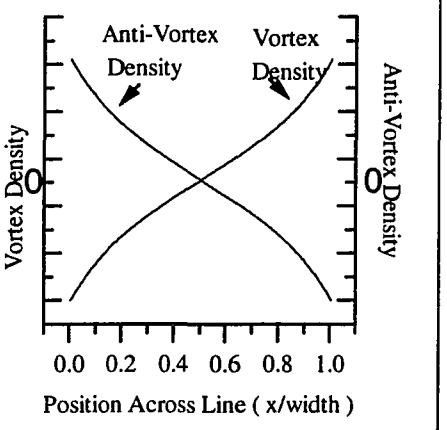

Fig. A-2 Magnetic Photoresponse of an Nb-Al Array vs Temperature

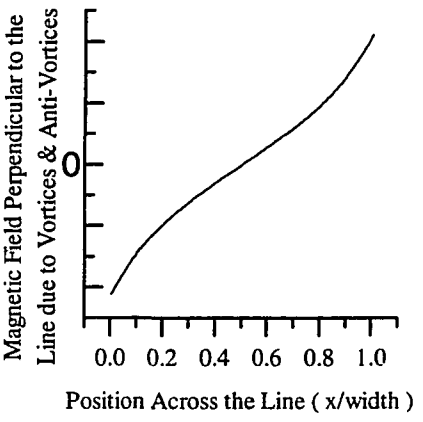

Fig. A-3 Magnetic Photoresponse of an Nb-Al Array vs Temperature

For the situation where the number of vortices leaving out an edge is equal to the number of antivortices entering that edge, or vise versa, $\gamma = an_0$ and the number of vortices and antivortices are constant and equal to one another. The magnetic field due to vortices in this case would be zero.

APPENDIX B

Calculation of Flux Transmission Through a Double Flux Transformer

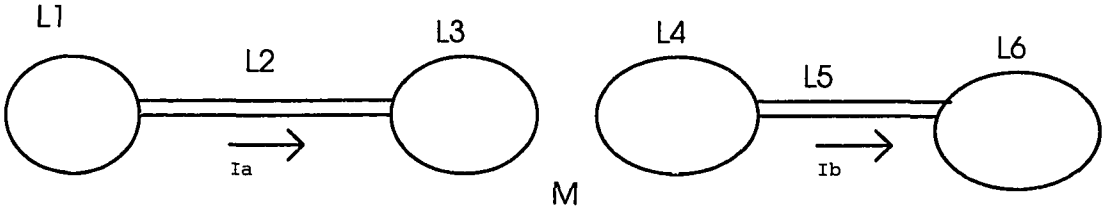

Boundary Conditions:

1) $Ia*L1 + \Phi 1ex + Ia*L2 + \Phi 2ex + Ia*L3 + \Phi 3ex = 0$
2) $Ib*L4 + \Phi 4ex + Ib*L5 + \Phi 5ex + Ib*L6 + \Phi 6ex = 0$
3) $M = \Phi 4ex / (Ia*L3) = \Phi 3ex / (Ib*L4)$

Let Φ_X = the total flux through L_X and Φ_{Xex} = the total external flux through L_X. This calculation is for the case of an ideal flux transformer with $\Phi_{2ex} = \Phi_{5ex} = 0$. In addition, to simplify the problem it will be assumed that no external flux is induced on L_6, giving $\Phi_{6ex} = 0$. The goal is then to find I_b*L_6/Φ_{1ex}.

Combining 1 & 3 and 2 & 3 gives

1) $Ia*L1 + \Phi 1ex + Ia*L2 + Ia*L3 + M*Ib*L4 = 0$
2) $Ib*L4 + M*Ia*L3 + Ib*L5 + Ib*L6 = 0$

or

1) $Ia*(L1 + L2 + L3) + \Phi 1ex + M*Ib*L4 = 0$
2) $Ib*(L4 + L5 + L6) + M*Ia*L3 = 0$

Solving 1) for I_a and substituting into 2) gives

$$Ia = - \frac{\Phi 1ex + M*Ib*L4}{L1 + L2 + L3}$$

$$Ib*(L4 + L5 + L6) - \frac{M*L3*(\Phi 1ex + M*Ib*L4)}{L1 + L2 + L3} = 0$$

then

$$Ib = \frac{\frac{M*L3*(\Phi 1ex + M*Ib*L4)}{L1 + L2 + L3}}{(L4 + L5 + L6)}$$

$$Ib = \frac{\frac{M*L3*\Phi 1ex}{L1 + L2 + L3}}{(L4 + L5 + L6)} + \frac{M*M*L3*L4*Ib}{(L1 + L2 + L3)*(L4 + L5 + L6)}$$

$$Ib = \frac{\frac{M*L3*\Phi 1ex}{\frac{L1 + L2 + L3}{(L4 + L5 + L6)}}}{1 - \frac{M*M*L3*L4}{(L1 + L2 + L3)*(L4 + L5 + L6)}}$$

$$Ib = \frac{\frac{M*L3*\Phi 1ex}{L1 + L2 + L3}}{L4 + L5 + L6 - \frac{M*M*L3*L4}{L1 + L2 + L3}}$$

$$Ib = \frac{M*L3*\Phi 1ex}{(L4 + L5 + L6)(L1 + L2 + L3) - M*M*L3*L4}$$

$$\frac{L6 \cdot Ib}{\Phi 1ex} = \frac{M \cdot L3 \cdot L6}{(L4 + L5 + L6)(L1 + L2 + L3) - M \cdot M \cdot L3 \cdot L4}$$

The above expression gives the efficiency of a pair of flux transformers, as used in the gradiometer experiments.

BIBLIOGRAPHY (Alphabetical)

A. A. Abrikosov, Soviet Phys. - JETP **5**, 1174 (1957)

S. N. Artemenko and Yu. I. Latyshev, Mod. Phys. Lett. B **6**, 367 (1992)

Y. Avishi and Y.B. Band, Phys. Rev. Lett. **66**, 1761 (1991)

Peter A. Bancel and K.E. Gray, Phys. Rev. Lett. **46**, 148 (1981)

John Bardeen and M.J. Stephen, Phys. Rev. l **40**, A1197 (1965)

H.A. Blackstead, D.B. Pulling, and C.A. Clough, Phys Rev. B **44** (1991)

L.N. Bulaevskii, S.V. Meshkov, and D. Feinberg, Phys. Rev. B **43**, 3728 (1991)

Y. Cai, P.L. Leath, and Z. Yu, Phys. Rev. B **49**, 4015 (1994)

G.L. Carr, M. Quijada, D.B. Tanner, C.J. Hirschmugl, G.P. Williams, S. Etemad, F. DeRosa, T. Venkatesan, B. Dutta, D. Hemmick, and X. Xia, SPIE **1292**, 187 (1990)

S.Q. Chen, W.J. Skocpol, E. DeObaldia, M. O'Malley, and P.M. Mankiewich, Phys. Rev. B **47**, 2936 (1993)

John Clarke, Wolfgang M. Goubau, and Mark B. Ketchen, J. Low Temp. Phys. **25**, 99 (1976)

John R. Clem, Physica A **200**, 118 (1993)

M.B. Cohn, M.S. Rzchowski, S.P. Benz, and C.J. Lobb, Phys. Rev. B **43**, 12823 (1991)

J.R. Cooper, S.D. Obertelli, A. Carrington, J.W. Loram and W.Y. Liang, Physica C **185**, 1265 (1991)

J.C. Culbertson, U. Strom, S. A. Wolf, P. Skeath, E.J. West, and W.K. Burns, Phys. Rev. B **39**, 12359 (1989)

W.R. Donaldson, A.M. Kadin, P.H. Ballentine, and R. Sobolweski, Appl. Phys. Lett. **54**, 2470 (1989)

K. Enpuku, R. Cantor, and H. Koch, J. Appl. Phys. **71**, 2338 (1992)

A. T. Fiory, A.F. Hebard, and W.I. Glaberson, Phys. Rev. B **28**, 5075 (1983)

N. Fujimaki , Y. Okabe, and S. Okamura, J. Appl. Phys. **52**, 912 (1981)

J.C. Garland, D.J. VanHarlingen, Phys. Rev. Lett. **55**, 2047 (1985)

G. L. Garr, D. R. Karecki, and S. Perkowitz, J. Appl. Phys. **55**, 3894 (1984)

B. I. Halperin and David R. Nelson, J. Low Temp. Phys. Vol. **36**, 599 (1979)

A.F. Hebard and S. Nakahara, Appl. Phys. Lett. **41**, 1132 (1982)

F.A. Hegmann, J.S. Preston, Phys. Rev. Lett. **48**, 16023 (1993)

Baruch Horovitz, Phys. Rev. Lett. **67**, 378 (1991)

B. Janossy, D. Prost, S. Pekker, and L. Fruchter, Physica C **181**, 51 (1991)

B. Janossy, H. Gu, R. Cabanel, L. Fruchter, Physica C **193**, 344 (1992)

Mark Johnson, Appl. Phys. Lett. **59**, 1371 (1991)

A.M. Kadin, M. Leung, A.D. Smith, and J. M. Murduck, Appl. Phys. Lett. **57**, 2847 (1990)

A.M. Kadin, J. Appl. Phys. **68**, 5741 (1990)

A. M. Kadin, M. Leung and A. D. Smith, Phys. Rev. Lett. **65**, No. 25, 3193 (1990)

A.M. Kadin, W.R. Donaldson, J.H. Scofield, and L. Bajuk, SPIE **1292**, 176 (1990)

A. Kleinhammes, C.L. Chang, W.G. Moulton, and L.R. Testardi, Phys. Rev. B **44**, 2313 (1991)

A.E. Koshelev, G. Yu Logvenov, V.A. Larkin, V.V. Ryazanov, and K. Ya. Soifer, Physica C **177**, 129 (1991)

J. M. Kosterlitz and D. J. Thouless, J. Phys. C **6**,1181 (1973)

H. S. Kwok, L. Shi, J.P. Zheng, S.Y. Dong, Y. Pang, and P. N. Prasad, SPIE **1394**, 196 (1990)

P.L. Leath and W. Xia, Phys. Rev. B **44**, 9619 (1991)

Hu Jong Lee, D.A. Rudman, and J.C. Garland, Phys. Rev. Lett. **55**, 2051 (1985)

M. Leung, U. Strom, J. C. Culbertson, J.H. Claassen, S. A. Wolf, and R. W. Simon, Appl. Phys. Lett. **50**, 1691 (1987)

C.G. Levey, S. Etemad, and A. Inam, Appl. Phys. Lett. ., 126 (1992)

M.Lindgren, V. Trifonov, M. Zorin, M. Danerud, D. Winkler, B.S. Karasik, B N. Gol'tsman, E.M. Gershenzon, Appl. Phys. Lett. **64**, 3036 (1994)

Petter Minnhagen and Peter Olsson, Phys Rev. B **44**, 4503 (1991)

P. Minnhagen and P. Olsson, Physica Scripta T42, **29** (1992)

R.S. Nebosis, M.A. Heusinger, W. Schatz, K.F. Renk, G.N. Gol'tsman, B.S. Karasik, A.D. Semenov, and G.M. Gershenzon, Optics Lett. **18**, 96 (1993)

E.H. Rhoderick, Nature **194**, 1167 (1962)

D.J. Resnick, J.C. Garland, J.T. Boyd, S. Shoemaker, and R.S. Newrock, Phys. Rev. Lett. **47**, 1542 (1981)

A.N. Samus, A.F. Popkov, V.I. Makhov, I.B. Krynetskii, I.V. Zolotukhin, and A.K. Zevezdin, Superconductivity **4,** 1229 (1991)

Gi. Schneider, P.G.Huggard, T. O'Brien, P. Lemoine, W. Blau, and W. Prettl, Appl. Phys. Lett. **60**, 648 (1992)

A.D. Semenov, G.N. Gol'tsman, I.G. Gogidze, A.V. Sergeev, P.T. Lang, K.F. Renk, Appl. Phys. Lett. **60**, 903 (1992)

R.W. Simon, B.J. Dalrymple, D. Van Vechten, W.W. Fuller, and S.A. Wolf, Phys. Rev. B **36**, 1962 (1987)

Keiichi Tanabe, Syugo Kubo, Youichi Enomoto, Hidefumi Asano, and Akihiko Yamaji, Jpn. J. of Appl. Phys. **30**, L110 (1990)

Tinkham, Introduction to Superconductivity, Krieger Publishing Co. p. 151 (1975)

Tinkham, Introduction to Superconductivity, Krieger Publishing Co. p. 149 (1975)

J.M. Triscone, O. Fischer, O. Brunner, L. Antognazza, A.D. Kent, and M.B. Karkut, Phys. Rev. Lett. **64**, 804 (1990)

P. Umadeve Muralidharan, T.R.Ramamohan, Phys Stat. Sol (a) **130**, 153 (1992)

B.J. Van Wees, Phys. Rev. B **44**, 2264 (1991)

L. N. Vu and D.J. VanHarlingen, Private communication

T. Wang, K.M. Beauchamp, D.D. Berkley, B.R. Johnson, J. X. Liu, J. Xhang, and A.M. Goldman, Phys. Rev. B **43**, 8623 (1991)

Hans Weber, Henrik Jeldotft Jensen, Phys. Rev. B **44**, 454 (1991)

R. Weinstein, In-Gann Chen, J. Liu, D. Parks, V. Selvanamickam and K. Salama, Appl. Phys. Lett. **56**, 1475 (1990)

K. Weiser, U. Strom, S. A. Wolf, and D. U. Gubser, J. Appl. Phys. **52**, 4888 (1981)

VITA

Joseph Philip Walko II was born on July 8, 1965 in Connecticut. He began his formal education in September, 1970, graduating magna cum laude from Potsdam College of the State University of New York in May 1987 with a B.A. in physics. From there he went to Purdue, and after passing the qualifying exam transferred to the University of Illinois at Urbana-Champaign where he got his M.S. in physics in December 1989.